Supplemental material to this article can be found at:
http://dmd.aspetjournals.org/content/suppl/2021/06/18/dmd.121.000428.DC1
1521-009X/50/6/781–797$35.00
https://doi.org/10.1124/dmd.121.000428
Drug Metabolism and Disposition
Drug Metab Dispos 50:781–797, June 2022

Minireview

The Nonclinical Disposition and Pharmacokinetic/Pharmacodynamic Properties of *N*-Acetylgalactosamine–Conjugated Small Interfering RNA Are Highly Predictable and Build Confidence in Translation to Human

Robin McDougall[1], Diane Ramsden[1], Sagar Agarwal, Saket Agarwal, Krishna Aluri, Michael Arciprete, Christopher Brown, Elena Castellanos-Rizaldos, Klaus Charisse, Saeho Chong, Joseph Cichocki, Kevin Fitzgerald, Varun Goel, Yongli Gu, Dale Guenther, Bahru Habtemariam, Vasant Jadhav, Maja Janas, Muthusamy Jayaraman, Jeffrey Kurz, Jing Li, Ju Liu, Xiumin Liu, Steven Liou, Chris Maclauchlin, Martin Maier, Muthiah Manoharan, Jayaprakash K. Nair, Gabriel Robbie, Karyn Schmidt, Peter Smith, Christopher Theile, Akshay Vaishnaw, Scott Waldron, Yuanxin Xu, Xuemei Zhang, Ivan Zlatev, and Jing-Tao Wu

Alnylam Pharmaceuticals, Cambridge, Massachusetts

Received February 16, 2021; accepted June 10, 2021

ABSTRACT

Conjugation of oligonucleotide therapeutics, including small interfering RNAs (siRNAs) or antisense oligonucleotides, to *N*-acetylgalactosamine (GalNAc) ligands has become the primary strategy for hepatocyte-targeted delivery, and with the recent approvals of GIVLAARI (givosiran) for the treatment of acute hepatic porphyria, OXLUMO (lumasiran) for the treatment of primary hyperoxaluria, and Leqvio (inclisiran) for the treatment of hypercholesterolemia, the technology has been well validated clinically. Although much knowledge has been gained over decades of development, there is a paucity of published literature on the drug metabolism and pharmacokinetic properties of GalNAc-siRNA. With this in mind, the goals of this minireview are to provide an aggregate analysis of these nonclinical absorption, distribution, metabolism, and excretion (ADME) data to build confidence on the translation of these properties to human. Upon subcutaneous administration, GalNAc-conjugated siRNAs are quickly distributed to the liver, resulting in plasma pharmacokinetic (PK) properties that reflect rapid elimination through asialoglycoprotein receptor–mediated uptake from circulation into hepatocytes. These studies confirm that liver PK, including half-life and, most importantly, siRNA levels in RNA-induced silencing complex in hepatocytes, are better predictors of pharmacodynamics (PD) than plasma PK. Several in vitro and in vivo nonclinical studies were conducted to characterize the ADME properties of GalNAc-conjugated siRNAs. These studies demonstrate that the PK/PD and ADME properties of GalNAc-conjugated siRNAs are highly conserved across species, are largely predictable, and can be accurately scaled to human, allowing us to identify efficacious and safe clinical dosing regimens in the absence of human liver PK profiles.

SIGNIFICANCE STATEMENT

Several nonclinical ADME studies have been conducted in order to provide a comprehensive overview of the disposition and elimination of GalNAc-conjugated siRNAs and the pharmacokinetic/pharmacodynamic translation between species. These studies demonstrate that the ADME properties of GalNAc-conjugated siRNAs are well correlated and predictable across species, building confidence in the ability to extrapolate to human.

Introduction

RNA interference (RNAi) is an intrinsic mechanism of post-transcriptional gene silencing mediated by double-stranded small oligonucleotides, 21–25 nucleotides in length, known as short interfering RNA (siRNA) (Fire et al., 1998; Meister and Tuschl, 2004). This catalytic process begins with loading duplex siRNA into the RNA-induced silencing complex (RISC) and removal of passenger (sense) strand to generate functional RISC containing only the guide (antisense) strand. RISC-loaded guide strands then bind to a complementary target mRNA through Watson-Crick base pairing, triggering the endonucleolytic cleavage of the target mRNA opposite the guide nucleotides at position 10–11 from the 5′ end. After nearly two decades of research and development, ONPATTRO, a partially modified siRNA encapsulated in a lipid nanoparticle, became the first RNAi therapeutic to receive marketing authorization in 2018.

Direct conjugation of the siRNA to a multivalent *N*-acetylgalactosamine (GalNAc) ligand combined with extensive chemical modifications

This work was supported by Alnylam Pharmaceuticals.
The authors have no conflict of interest but are current or former employees of Alnylam Pharmaceuticals.
[1]R.M. and D.R. contributed equally to this work.
dx.doi.org/10.1124/dmd.121.000424.
This article has supplemental material available at dmd.aspetjournals.org.

to stabilize the siRNA allowed for selective targeting of hepatocytes in the liver through the asialoglycoprotein receptor (ASGPR) and has been transformative for liver-directed therapeutic oligonucleotides (Nair et al., 2014). An early generation of GalNAc-conjugated siRNA, with only a few further modifications designated as standard template chemistry (STC), achieved clinical proof of concept but required a high and frequent dose regimen (Zimmermann et al., 2017). Subsequent design improvements, which include the substitution of the two terminal phosphodiester linkages at the antisense 3′ and 5′ ends and the sense strand 5′ end with phosphorothioate linkages, led to the enhanced stabilization chemistry (ESC) design, with improved metabolic stability and potency enabling a reduction in total dose amount required and allowing for less frequent administration (Nair et al., 2017). GIVLAARI, the first GalNAc-conjugated siRNA with ESC design, received regulatory approval in 2019. It is dosed at 2.5 mg/kg monthly by subcutaneous injection. Continued refinement of the chemical modification pattern led to the development of advanced ESC designs with increased metabolic stability (Foster et al., 2018), and inclusion of seed destabilizing modifications, like glycol nucleic acid, provides improved specificity, designated as ESC+ design (Janas et al., 2018). These advances have resulted in prolonged duration of target protein reduction in nonclinical studies and investigational clinical studies (Ray et al., 2020). Vutrisiran, an advanced ESC GalNAc-conjugated siRNA currently in phase 3 clinical development, demonstrates sustained pharmacodynamic (PD) effect lasting up to 10 months after a single 25-mg s.c. dose in healthy volunteers (Habtemariam et al., 2021).

Unlike traditional small-molecule drugs, siRNAs are large hydrophilic molecules. The two complementary strands of siRNA form double-helical structures of 19–21 base pairs with a molecular mass of ∼14,000 kDa. Their polyanionic backbone and hydrophilic character prevent passive uptake across cell membranes and therefore require specialized delivery solutions to achieve adequate cellular uptake. Over the past several years, knowledge of nonclinical ADME properties has been accumulated with dozens of GalNAc-conjugated siRNAs, including STC, ESC, Advanced ESC, and ESC+ designs.

Data generated in nonclinical studies of GalNAc-conjugated siRNAs suggest that after subcutaneous administration, rapid hepatic uptake is followed by slow metabolism and clearance from the liver (Nair et al., 2017; Zimmermann et al., 2017). As such, plasma concentrations are transient and not directly reflective of the prolonged duration of PD. The maximum plasma concentration after subcutaneous administration of GalNAc-conjugated siRNA in all nonclinical species was typically achieved around 0.25 hours to 2 hours postdose, with the last detectable concentration in plasma, above the lower limit of quantification, observed between 4 and 12 hours, indicating rapid and efficient hepatic uptake (Nair et al., 2017; Foster et al., 2018). This was reproducible across different siRNA-conjugate chemistries and various nonclinical species. In contrast, peak liver concentrations in mice, rats, and monkeys are generally observed between 2 and 8 hours post–subcutaneous administration, which highlights the rapid and efficient uptake of GalNAc-siRNA. Recent work highlights an acidic intracellular depot that contributes significantly to the durable PD effect (Brown et al., 2020). This work demonstrates that the high metabolic stability of current-generation GalNAc-conjugated siRNAs in intracellular compartments results in continuous and sustained release of functionally active siRNAs into cytoplasm, where they can load into RISC and elicit a prolonged PD effect.

The current series of nonclinical ADME investigations have been conducted over years to support the continuous development of GalNAc-siRNA. The goal of this works is to summarize the knowledge gained with respect to the absorption, distribution, metabolism, and excretion (ADME) properties; to compare and contrast between molecules containing different sequences but similar chemical modifications; and to provide a reference to work we have completed that aimed to describe the translation between nonclinical PK properties and human.

Materials and Methods

Chemicals and Reagents. Clarity OTX lysis loading buffer and Clarity OTX 96-well solid-phase extraction plates were obtained from Phenomenex (Torrance, CA). Optima liquid chromatography–mass spectrometry (LC-MS)-grade acetonitrile and water, 6× electrophoretic mobility shift assays (EMSAs) gel loading solution, and SYBR gold nucleic acid gel stain were purchased from Thermo Scientific (Waltham, MA), and 1,1,1,3,3,3-hexafluoro-2-propranol (HFIPA), *N*,*N*-diisopropylethylamine (DIEA), ammonium acetate, ammonium bicarbonate, and tetrahydrofuran were purchased from Millipore Sigma (Darmstadt, Germany). *β*-*N*-acetylglucosaminadase, Nuclease P1, and glycobuffer 1 were purchased from New England Biolabs. Tris-borate-EDTA (10%) gel was from Bio-Rad Laboratories (CA). Oligonucleotides were synthesized at Alnylam by solid-phase synthesis using an RNA synthesizer. Sterling solvents/reagents from Glen Research, 500-Å controlled pore glass solid supports from Prime Synthesis, and 2′-OMe, 2′-F nucleoside 3′-phosphoramidites from Hongene were all used as received. Low-water-content acetonitrile was purchased from EMD Chemicals. Male hepatocytes were purchased from BioIVT (Westbury, NY). All siRNAs had high-performance liquid chromatography purity of >90%, and all tritium-labeled siRNAs had high-performance liquid chromatography radiopurity of >96% and a tritium-specific activity of >250 μCi per mg of siRNA. The tritium-specific activity was measured using a Hidex 300 SL liquid scintillation counter (Lablogic).

GalNAc-siRNA Synthesis and Selection Criteria for Inclusion in Specific Studies. Synthesis of GalNAc-siRNAs used in this analysis was conducted as previously described (Nair et al., 2014). The general chemical modifications previously disclosed for late-stage development siRNA, including revusiran, givosiran, and lumasiran, were used in all GalNAc-siRNAs described throughout this report (Shen and Corey, 2018) and are depicted in Fig. 1; for cases in which glycol nucleic acid was used, the design was consistent with those published (Schlegel et al., 2017). For assessment of sex-dependent differences in GalNAc-siRNA PK, all available data obtained in male and female animals were included in the analysis. For mechanistic studies including in vitro confirmation of duplex metabolism, siRNA2 was used as the surrogate GalNAc-siRNA, as it is reflective of the ESC design and has a complete data package available (including radiolabeled ADME, QWBA, and metabolite assessment including determination of metabolite contributions to pharmacology). All data available in the 5/6 nephrectomy model and rat ADME/QWBA studies are included. The siRNA used in these studies was decided based on the stage of individual projects and project needs to inform their development. All studies describe data generated with GalNAc-siRNAs, which were randomly anonymized through serial numbering from 1 to 22. There are no data presented for siRNA10.

ABBREVIATIONS: ADME, absorption, distribution, metabolism and excretion; Ago2, protein argonaute-2; AS, antisense strand; ASGPR, asialoglycoprotein receptor; AS(N-1)3′, loss of a single nucleotide from the 3′ end of the antisense strand (also designated as 3′N-1); AUC, area under the curve; BDC, bile duct–cannulated; DIEA, *N*, *N*-diisopropylethylamine; EMSA, electrophoretic mobility shift assay; ESC, enhanced stability chemistry; ESC+, enhanced stability chemistry with stabilizing modifications; GalNAc, *N*-acetylgalactosamine; ^{3}H, tritium; HFIPA, 1,1,1,3,3,3-hexafluoro-2-propranol; IS, internal standard; LC-HRMS, liquid chromatography coupled with high-resolution mass spectrometry; LC-MS, liquid chromatography–mass spectrometry; LSC, liquid scintillation counting; MARG, microautoradiography; PCR, polymerase chain reaction; PD, pharmacodynamics; PK, pharmacokinetics; qPCR, quantitative PCR; QWBA, quantitative whole-body autoradiography; RISC, RNA-induced silencing complex; RNAi, RNA interference; RT-qPCR, real-time quantitative polymerase chain reaction; siRNA, small interfering RNA; STC, standard template chemistry; $t_{1/2}$, half-life; T_{max}, time at which maximal concentration was observed.

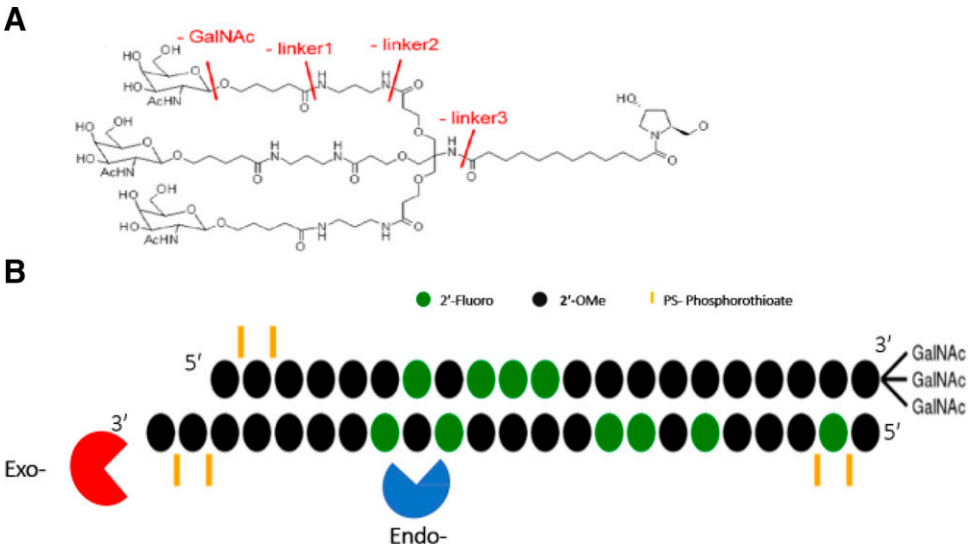

Fig. 1. Metabolic scheme of sense strand (A) and antisense strand (B). The sense strand contains three GalNAc moieties attached to a linker, which can undergo cleavage of the amide bonds at positions 1 (linker 1) through 3 (linker 3). The antisense strand (B) can undergo metabolism by exonucleases (red) that work on the end of the strand, resulting in release of mononucleotides, whereas endonucleases (blue) cleave internally and result in strands of varying lengths. The GalNAc-siRNAs evaluated in these series of studies contain consistent chemical modifications of the 2′ ribose including substitution of a fluoro (green) or O-methyl (black). The GalNAc in the ESC and above classes also contain phosphorothioate (PS) in place of phosphorodiester bonds in the six labeled positions (orange line). The earlier class of GalNAc-siRNAs that revusiran and siRNA20 are from, called STC, contain only two PS bonds at the overhang nucleotides in the antisense strand at the 3′ end.

In Vitro Metabolism of GalNAc-Conjugated siRNA. siRNA2 was incubated at 160 μg/ml with *β-N*-acetylglucosaminadase at 37°C for 0, 1, and 2 hours in glycobuffer 1. siRNA8 was incubated at 10 μg/ml with plated rat, monkey, and human hepatocytes. Samples were removed at designated time points and pooled for LC-MS analysis. Reactions were terminated by the addition of EDTA solution and frozen in liquid nitrogen, followed by lysis at room temperature in the presence of lysis loading buffer. The resulting samples were extracted on Clarity OTX SPE according to the manufacturer's instructions, and concentrations of antisense strand and sense strand were quantified by LC-MS.

In Vitro Metabolism of siRNA. siRNA2 duplex and single strands (antisense and sense strand) separately were incubated (16 and 6 μg/ml) with single-strand–specific nucleases including Nuclease P1. This nuclease acts on single strands from the 3′ direction. Enzyme incubations were conducted at three activity levels each, ranging from 0.2 to 400 units. Aliquots were removed for analysis after 15 and 60 minutes. Samples were analyzed by liquid chromatography coupled with high-resolution mass spectrometry (LC-HRMS) and were normalized to the matrix-only (containing no enzyme) control values. EMSAs were used to determine whether complementary antisense and sense strand, comprising siRNA2 or siRNA19, mixed at equivalent concentrations (8 μg/ml or 4.8 μg/ml), would form duplex in PBS and 99% human plasma.

Nonclinical In Vivo PK/PD Studies. All animal studies were conducted in accordance with local, state, and federal regulations as applicable and were approved by the Institutional Animal Care and Use Committee. Studies were conducted in male and female Sprague-Dawley rats, male and female CD1 and C57BL/6, and male and female cynomolgus monkeys from various contract research organizations (i.e., Charles River Laboratories, Covance). Typically, samples from three animals per group were used to describe plasma, tissue, and excretion (urine and feces) pharmacokinetic properties. For studies in mice and rats, composite profiles were obtained because of the large sample volumes needed for quantitation of siRNA levels. Studies in rats were conducted using animals at least 8 weeks of age with a target weight of 300–400 g at the initiation of dosing. Rodents were group-housed with up to three animals of the same sex and same dosing group together, with the exception of animals identified for urine collection, which were housed individually in metabolism cages for the duration of the urine collection period. All animals were provided enrichment activities. Chow was provided ad libitum, except during designated procedures, and water was freely available via automatic watering systems. Terminal blood samples were collected via jugular venipuncture or abdominal aorta (at least 0.5 ml) at designated time points into K_2EDTA-containing tubes for preparation of plasma. For studies in monkeys, naïve cynomolgus (*Macaca fascicularis*) originating from China that weighed between 2 and 4 kg with the target age of 2–4 years were used. Monkeys were socially housed (up to three animals of the same sex and dosing group together), except for directly after procedures or when used for collection of urine, enrichment activities were provided, food was offered twice daily, and water was available ad libitum. Monkeys were used as the pharmacologically relevant species with more relevant target phenotyping comparable to human. For pharmacodynamic analysis, up to 3 ml of blood was collected at time points spanning day 1 up to day 99. At designated time points (i.e., 0.25, 0.5, 1, 2, 4, 8, 12, and 24 hours postdose) target 1 ml of blood was removed via venipuncture into K_2EDTA tubes for preparation of plasma to support PK parameter estimation and metabolite profiling. To support derivation of liver PK parameters, liver biopsies (target 150–200 mg/biopsy) were removed from a single monkey per group per time point for quantitation of siRNA levels, and up to three biopsies were possible per animal. Samples were stored at −70°C until analysis. Studies in rat and monkey were conducted using various dose levels spanning from 0.03 mg/kg to 30 mg/kg, given as an intravenous bolus injection, infusion into a lateral tail vein, or through subcutaneous administration into the scapular or mid-dorsal areas. Historical knowledge related to the safety of this modality and the potency of PD observed during screening assays was used to design dose levels and regimens. Dose volume was limited to 1.5 ml/kg. When comparisons were made between groups to evaluate the statistical significance, a two-tailed, unpaired, Student's *t* test with unequal variance was used.

Assessing the Role of Renal Clearance Using 5/6 Nephrectomy Studies. Male Sprague-Dawley rats (5/6 nephrectomy and sham) were prepared as described previously (Kliem et al., 1996). In short, two-thirds of one kidney was removed, followed by a second surgery (3–7 days later) to remove the entire second kidney. Renal damage was confirmed by monitoring urinary excretion of protein, creatinine clearance, and histopathological examination. siRNA5, siRNA11, and siRNA14 were dosed approximately 4 weeks after sham or 5/6 nephrectomy surgery data from three to five rats per time point were combined for generation of composite PK profiles. Blood samples were typically collected (0.3 ml) at predose, 0.5, 2, 4, 8, 24, and 336 hours for preparation of plasma and generation of plasma PK parameters. Liver and kidney samples were collected at similar time points. Urine and feces were collected at time intervals of 0–4, 4–8, 8–24, 24–48, and 48–72 hours for siRNA quantitation. Student's *t* tests were used to evaluate whether any differences between sham-operated and 5/6 nephrectomized rats were significantly significant. The following parameters were assessed: daily clinical observations, body weight, clinical pathology (clinical chemistry), creatinine, and urine collection for chemistry and biomarkers. At the

end of the treatment period on days 2, 4, and 8, the animals were euthanized, and a complete macroscopic examination was performed. Liver and kidneys were weighed, and microscopic evaluation was conducted. A section of the liver (right lateral lobe) and half of the remaining kidney in the nephrectomized animals and half of the left kidney in the sham animals were frozen for test article concentration analysis.

Mass Balance and Excretion Studies in Rats. Tritiated siRNA was prepared as described in detail in the Supplemental Material. Male bile duct–cannulated (BDC) and femoral vein–cannulated Sprague-Dawley rats were used. Dose levels of 3 mg/kg were selected for siRNA2 and siRNA6, and 10 mg/kg was selected for siRNA20. The following samples were collected for analysis of excretion of radioactivity and mass balance. Urine samples were collected on dry ice at predose (overnight); 0–6, 6–12, and 12–24 hours postdose; and at 24-hour intervals through 1344 hours postdose. Feces samples were collected on dry ice predose (overnight); at 0–6, 6–12, and 12–24 hours postdose; and at 24-hour intervals through 1344 hours postdose. After each 24-hour excreta collection through 1344 hours postdose, with the exception of cage change days, cages were rinsed with water followed by a rinse with approximately 30 ml of ethanol:-deionized water (v:v, 1:1). Cage rinse samples were collected. At the time of each cage change and after the last excreta collection, cages were washed and wiped with at least 90 ml of Count-Off solution (equivalent to RadiacWash). The cage wash and cage wipe samples were collected for LSC analysis. In addition to the fecal and urine samples in the bile duct–cannulated rats, bile was also sampled for determining mass balance and excretion pathways. Bile samples were collected on dry ice from each animal at predose (overnight); at 0–6, 6–12, and 12–24 hours postdose; and at 24-hour intervals. Ultima Gold XR scintillation cocktail was used for samples analyzed directly. All samples were analyzed for radioactivity in Model2900TR or 2910TRliquid scintillation counters (Packard Instrument Company) for at least 5 minutes or 100,000 counts. Each sample was homogenized before radioanalysis (unless the entire sample was used for analysis). All samples were analyzed in triplicate (as applicable) if sample size allowed. Scintillation counting data (cpm) were automatically corrected for counting efficiency using the external standardization technique and an instrument-stored quench curve generated from a series of sealed quenched standards. A second set of duplicate or triplicate (as applicable) aliquots of bile, blood, plasma, and urine were dried and analyzed. The results were compared with original analysis results to determine the tritiated water content of each sample.

Quantitative Whole-body Autoradiography Studies in Rats. BDC and intact femoral vein–cannulated male Sprague-Dawley rats were used. Dose levels of 3 mg/kg were selected for siRNA2 and siRNA6, and 10 mg/kg was selected for siRNA20. The total amount of radioactivity administered was approximately 500 μCi/kg. As much blood as possible was collected from all animals via exsanguination (cardiac puncture). Blood was transferred into tubes to obtain plasma within 30 minutes of collection. One animal per time point was prepared for QWBA at staggered time points through 1344 hours (56 days) postdose. The carcasses were immediately frozen, and each carcass was stored at approximately −70°C. The pinna, limbs, hair (as necessary), and tail of each frozen carcass for QWBA were removed and frozen into a block, and a section set from each animal was prepared to be exposed on phosphorimaging screens for 7 days. Specified tissues, organs, and fluids were analyzed. Tissue concentrations were interpolated from each standard curve as nanocuries per gram and then converted to nanogram equivalents per gram on the basis of the test article specific activity. Tissue concentration data were determined if examination of the autoradiographs warranted analysis. Specified tissues, organs, and fluids were analyzed, and the tissue concentrations were interpolated from each standard curve as microcuries or nanocuries per gram (μCi/g or nCi/g).

Red Blood Cell Partitioning in Rat. Blood was mixed by inverting several times. Triplicate weighed aliquots of each blood sample (approximately 0.1 g) were removed for radioanalysis by LSC. A sufficient amount of commercial solubilizing agent was added to digest each sample. Samples were incubated for at least 1 hour at approximately 60°C. The samples were allowed to sit at least overnight to allow any foaming to dissipate. Ultima Gold XR scintillation cocktail was added, and the samples were shaken and analyzed by LSC. Additional duplicate weighed aliquots of blood were dried under a stream of nitrogen and reconstituted in water. A sufficient amount of commercial solubilizing agent was added to digest each sample. Samples were incubated for at least 1 hour at approximately 60°C. The samples were allowed to sit at least overnight to allow any foaming to dissipate. Ultima Gold XR scintillation cocktail was added, and the samples were shaken and analyzed by LSC. The remaining blood samples were centrifuged within 30 minutes of collection to separate plasma at 3000 rpm (1500*g*) for approximately 10 minutes at approximately 5°C. The resulting plasma was mixed, and duplicate weighed aliquots of each resultant plasma sample (approximately 0.1 g, as available) were removed for radioanalysis by LSC.

Microautoradiography Evaluation. A set of representative sections for each male rat (with internal standards for each section) were mounted on thin cardboard supports. The mounted sections were exposed to phosphorimaging screens. Remaining dose formulation spiked blood calibration standards at eight different concentrations were coexposed with all sections, and the images were used for calibrating the image analysis software. The exposed screens were scanned using a Typhoon FLA 9500 Phosphor Imager, and data were acquired as DensRFU/μm^2. The autoradiographic standard image data (calibration and internal standards) were sampled using MCID software to create a calibrated standard curve and to verify section thickness uniformity. Specified tissues, organs, and fluids were analyzed, and the tissue concentrations were interpolated from each standard curve as microcuries per gram (μCi/g or nCi/g). The concentrations were converted to nanogram equivalents of parent compound per gram of tissue based on the specific activity of the parent compound in the dosing formulation.

Evaluation of the Potential for Enterohepatic Recirculation to Impact Pharmacodynamics. Intact and bile duct–cannulated female Sprague-Dawley rats (n = 4/group) were dosed with 1 mg/kg siRNA11 followed by serial blood collections (0.3 ml) at predose, 24, 48, 72, 96, 120, 144, and 168 hours postdose. Bile and liver samples were also collected for potential analysis. Serum was prepared from whole blood for evaluation of the target present using a commercially available ELISA kit. Female rats were chosen because previous studies using siRNA11, at this dose level, demonstrated recovery of pharmacodynamic response within the time frame applied in this study.

In Vitro Investigation on the Potential for Truncation Metabolites to Contribute to Pharmacodynamics. For each duplex evaluated, the antisense strand was truncated from either the 5′ or 3′ end relative to the full antisense strand of siRNA2. Because the antisense strand is the active strand, the composition of the sense strand was not changed. As such, all duplexes were annealed to the full-length sense strand, the same sense strand employed in siRNA2 drug substance. Hep3B cells were transfected by adding 4.9 μl of Optimized Minimal Essential Medium plus 0.1 μl of LipofectAMINE RNAiMAX Transfection Reagent per well (catalog number 13778150; Invitrogen, Carlsbad, CA) to 5 μl of siRNA duplexes per well into a 384-well plate. The plate was incubated at room temperature for 15 minutes, and then 40 μl of Eagle's Minimum Essential Medium containing $\sim 5 \times 10^3$ cells was added to the siRNA mixture. Cells were incubated for 24 hours before RNA purification. Two separate experiments were performed at final duplex concentrations of 0.0016 and 0.16 μg/ml, respectively, and mRNA was assayed 24 hours after transfection by quantitative polymerase chain reaction (qPCR). Briefly, 2 μl of cDNA was added to a master mix containing 0.5 μl of glyceraldehyde 3-phosphate dehydrogenase (GAPDH) TaqMan Probe (Hs99999905), 0.5 μl of commercially available target probe, and 5 μl of LightCycler 480 Probes Master (catalog number 04887301001; Roche, Indianapolis, IN) per well in a 384-well plate (catalog number 04887301001; Roche). qPCR was done in a LightCycler 480 qPCR system (Roche) using the ΔΔ threshold cycle (relative quantitation) assay. Each duplex was tested in four independent transfections. To calculate relative fold change, data were analyzed using the ΔΔ threshold cycle (relative quantitation) method and normalized to assays performed with cells transfected with 10 nM nontargeting siRNA (i.e., mock transfected cells). Data are expressed as percentage of message remaining, and error is expressed as S.D. derived from the four transfection replicates.

Mass-Spectroscopic (LC-HRMS) Analysis. Identities and purities of oligonucleotides were confirmed by electrospray ionization mass spectroscopy and ion exchange high-performance liquid chromatography. The liquid chromatography-time of flight-mass spectrometry (LC-TOF-MS) assays quantified the concentrations of specific GalNAc-conjugated siRNAs by detecting the antisense strand and sense strand portions of the duplex. Samples were spiked with internal standard (IS), processed by solid-phase extraction, and analyzed using reversed-phase ultra-high-performance liquid chromatography with turbo ion spray TOF-MS detection. Accurate masses of 10 ions for each strand of the analyte, sense, and antisense and each strand of the IS, sense, and antisense were monitored in the negative ionization mode. The peak area for the analyte or IS was the sum of the response from the respective 10 ions. The peak area ratios of the respective

analyte-sense/IS-sense and analyte-antisense/IS-antisense single strands were used. The detection limit for LC-HRMS detection was typically 10 ng/ml or 100 ng/g for plasma and tissue levels, respectively. Prior to using analytical methods, to support these nonclinical investigations, the methods were validated or qualified according to the recommendations set forth by regulatory bodies. Standard methods, instrumentation, columns, and IS were used as previously published (Li et al., 2019; Liu et al., 2019).

Quantification of siRNA Stem-Loop Reverse Transcription-Quantitative Polymerase Chain Reaction (SL-RT-qPCR). Quantitation of siRNA concentrations was conducted by diluting samples with an equivalent volume of PBS with Triton X (0.25% Triton X-100) or, in the case of tissue samples, reconstituting 10 mg of powdered tissue in 1 ml of PBS with Triton X. Diluted samples were incubated at 95°C for 10 minutes, vortexed, and immediately placed on ice for 10 minutes and then centrifuged for 10 minutes at 16,000*g* at 4°C. Supernatants were transferred to DNase/RNase-free tubes and analyzed immediately or frozen until analysis. Prior to stem-loop PCR, described below, a minimum of 20 μl of sample (plasma or tissue) was transferred into a 96-well plate and heated at 95°C for 10 minutes to allow duplex denaturing removal of secondary structures.

The general strategies previously published were employed to design primers and probes using a TaqMan-based approach (Chen et al., 2005; Landesman et al., 2010; Castellanos-Rizaldos et al., 2020). In short, the TaqMan MicroRNA Reverse Transcription Kit was used according to the manufacturer's recommendations under the following conditions: 5 μl of the denatured sample/standard/quality control was added to 10 μl of the reverse transcription reaction mixture containing 1× buffer, 1× reverse transcriptase, RNase inhibitor, stem-loop oligonucleotide, and water, and deoxyribonucleotide triphosphate (dNTP) reactions were incubated at 16°C for 30 minutes, followed by 42°C for 30 minutes, and were then inactivated at 85°C for 5 minutes. qPCR was performed on a ViiA 7 Real-Time PCR System using a 384-well block and TaqMan Fast advanced master mix following the manufacturer's protocols.

Quantification of RISC-Loaded siRNA. RISC-loaded siRNA (antisense strand) quantification using stem-loop RT-qPCR following Ago2 immunoprecipitation from liver samples was conducted as reported previously (Castellanos-Rizaldos et al., 2020). Processed liver samples were resuspended to 100 mg/ml in prechilled lysis buffer (50 mM Tris-HCl, pH 7.5, 150 mM NaCl, 2 mM EDTA, 0.5% Triton X-100) supplemented with one tablet of cOmplete Mini, EDTA-free protease inhibitor cocktail, and 1 mM phenylmethanesulfonyl fluoride. Samples were precleared using QAE-Sephadex R A-50 resin and subjected to Ago2 immunoprecipitation by incubation with anti-mouse Ago2 and normal mouse IgG as a control using Protein G Dynabeads (ThermoFisher Scientific). RISC-loaded siRNA was subsequently quantified by the stem-loop RT-qPCR approach described above.

Absolute Quantitation and Metabolite Profiling from Cell Lysate, Plasma, and Tissue Samples. Absolute quantitation of concentrations of specific siRNA in cell lysates, plasma, tissue, urine, and fecal samples and metabolite profiling were performed using a Dionex liquid chromatography system coupled to Q Exactive mass spectrometer (Thermo scientific Waltham MA). Solid-phase extraction using Clarity OTX 96-well plates was used to clean up samples before LC-MS analysis (Rudge et al., 2011). The 1% HFIPA/0.1% DIEA with 10 μM EDTA in water and 0.075% HFIPA/0.0375% DIEA with 10 μM EDTA in 65/35 acetonitrile/water were used as mobile phase A and B, respectively. LC-MS analysis for siRNA was performed either using t-sim or tandem mass spectrometry (MS/MS) mode and used a gradient reaching 40% B in 4 minutes or up to 20% B in 20 minutes for quantitation and metabolite profiling, respectively. Quantitation of parent siRNA (full-length antisense strand) and the potential major antisense metabolite AS(3′N-1) was conducted using Thermo Quan browser with a calibration curve ranging from 10 to 5000 ng/ml, and metabolite profiling of siRNA was performed using ProMass (Hail et al., 2004) (Novatia, Newtown, PA). Relative percentages of metabolites were calculated using peak intensities relative to total intensity within the sample. Metabolites were confirmed by manual evaluation of MS2 when available.

mRNA Quantitation for Pharmacodynamic Evaluations. Total mRNA was isolated and reverse transcribed into cDNA as previously described (Foster et al., 2018). qPCR reactions were performed using gene-specific TaqMan assays for each target gene of interest against representative species.

PK and PD Analysis. Pharmacokinetic parameters were calculated using noncompartmental analysis in Phoenix WinNonlin 7.0. Pharmacodynamics were evaluated by measuring target mRNA levels in liver samples or protein levels in serum using qPCR or ELISA as previously described (Foster et al., 2018).

Results

GalNAc-Conjugated siRNAs Retain Their Duplex Structure in Circulation. The direct determination of double-stranded versus single-stranded siRNAs in biologic matrices using LC-HRMS is technically challenging, as typical experimental conditions employed during LC-HRMS analysis would generally denature a double-stranded siRNA into its single strands. Thus, a series of experiments were conducted to evaluate whether the two strands stayed as a duplex in circulation and whether the concentration of one strand would represent the other strand as well as the duplex. Initially, Nuclease P1, a mixture of nucleases known to degrade RNA and DNA, were incubated with single strands and/or duplex siRNA. As depicted in Supplemental Table 1, the duplex was stable under all test conditions, whereas single strands (both sense and antisense) were quickly metabolized by Nuclease P1. This in vitro experiment suggested that the sense and antisense strands are likely not stable in circulation unless present as a duplex. Further in vivo experiments confirmed that both sense and antisense strand concentrations were typically represented at a 1:1 ratio across rat, monkey, and human plasma over extended periods of time (Fig. 2, A and B). The plasma pharmacokinetic parameters and the corresponding figures demonstrate no significant differences in derived parameters, as determined with a two-tailed, unpaired, Student's *t* test with unequal variance. At similar dose levels, the plasma C_{max} (ng/ml) values are consistent across species (Fig. 2A), but the AUC (h*ng/ml) in human is higher than what is observed in rat and monkey (Fig. 2, A and B). Comparison of exposures between siRNA1 and siRNA5 demonstrates that the exposure is consistent between these GalNAc-siRNAs. siRNA1 represents a newer chemistry containing a glycol nucleic acid, whereas siRNA5 is an advanced ESC GalNAc-siRNA. In addition, separate EMSA studies show that both siRNA2 and siRNA19 would form duplexes in PBS and/or plasma (siRNA19 only) when sense and antisense strands were combined at equivalent ratios (Supplemental Fig. 1). Taken together, these data strongly suggest that GalNAc-conjugated siRNAs stay as a duplex in circulation and that the measured levels of antisense strand are representative of intact duplex.

Absorption. An evaluation of sex dependence on plasma PK parameters was performed after dosing of five and seven different GalNAc-conjugated siRNAs in rats or cynomolgus monkeys, respectively (Table 1). The results demonstrated comparable C_{max} (ng/ml), AUC_{last} (h*ng/mL), T_{max} (h), $t_{1/2}$ (h), and percentage of dose observed in plasma at C_{max} between males and females of both rats and monkeys, with no statistically significant difference as measured using a two-tailed, unpaired, Student's *t* test with unequal variance (Table 1). The plasma PK in rats, monkeys, and humans increased in a dose-proportional manner at doses up to 10 mg/kg and are well correlated, confirming that human plasma PK can be predicted through allometric scaling (Fig. 2, C and D). Dose levels $>$ 10 mg/kg begin to show greater than dose-proportional increases, as exemplified by comparing the AUC across increasing dose levels: human (Fig. 2E) and monkey (Fig. 2F). This is likely due to transient saturation of ASGPR-mediated uptake clearance, which leads to increased plasma exposure. After subcutaneous injection, GalNAc-conjugated siRNA is absorbed quickly from the injection site and subject to rapid clearance from plasma (dominated by ASGPR-mediated uptake into the liver), with plasma C_{max} typically observed between 0.2 and 12 hours and plasma half-life less than 5 hours in rat and 10 hours in monkey and human (Fig. 2, A and B; Table 1). At plasma T_{max}, less than 1% of the subcutaneously injected dose resides in the plasma (scaling plasma concentration by

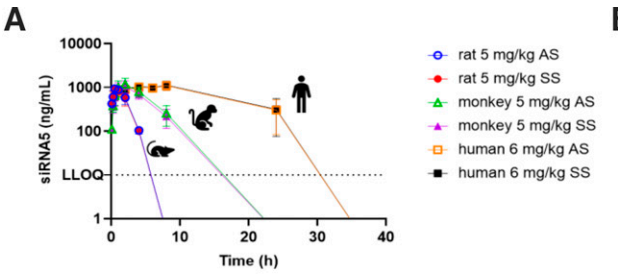

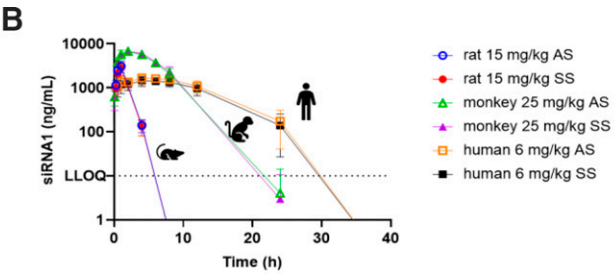

Parameter	rat		monkey		human	
	AS	SS	AS	SS	AS	SS
T_{max} (h)	0.5	0.5	2	2	8	8
C_{max} (ng/mL)	936	902	1180	1070	1100	1130
AUC (h*ng/mL)	2170	2060	5780	5120	18,670	19,200

Parameter	rat		monkey		human	
	AS	SS	AS	SS	AS	SS
T_{max} (h)	1	1	2	2	4	4
C_{max} (ng/mL)	3110	2830	6710	6740	1670	1450
AUC (h*ng/mL)	7160	6460	53,700	57,100	24,600	21,600

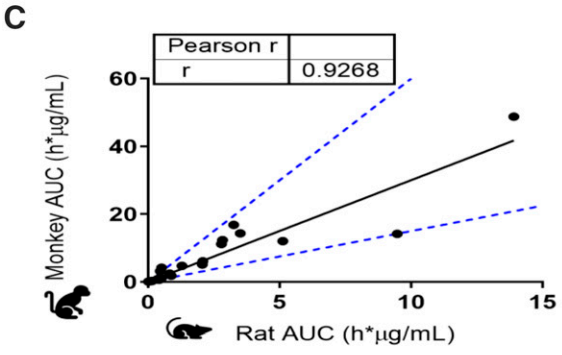

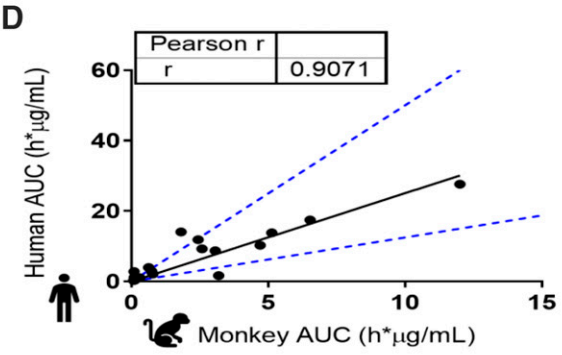

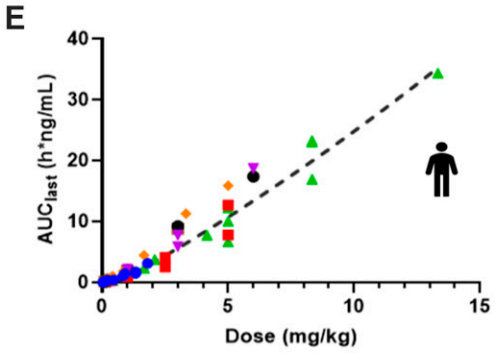

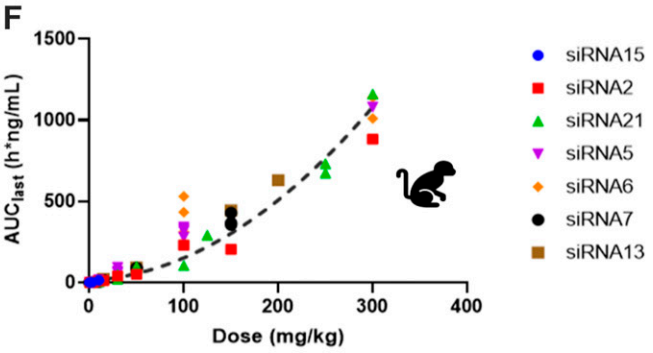

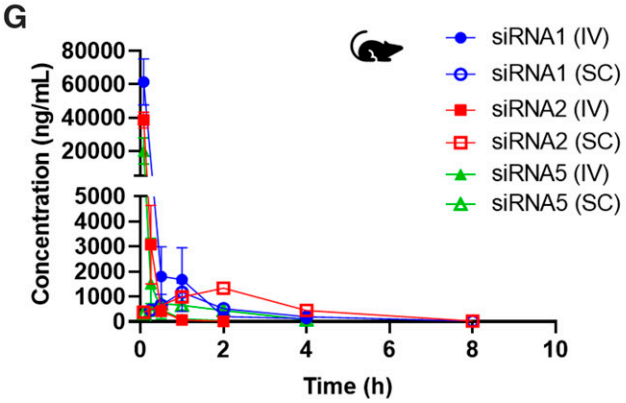

siRNA	AUC (h*ng/mL)		%F
	IV	SC	
1 (10 mg/kg)	10000	2640	26.4
2 (10 mg/kg)	5670	3230	57.0
5 (5 mg/kg)	3090	1650	53.4

Fig. 2. Mean ± S.D. siRNA5 (A) or siRNA1 (B) duplex plasma concentration-time profiles based on AS and sense strand (SS) after a single subcutaneous administration of varying but similar dose levels in rat, monkey, and human. The data are plotted as the mean and S.D. (error bars) of n = 4, 6, or 10 data points per time point. The lower limit of quantitation (LLOQ) for assay was 10 ng/ml (dashed line). The PK parameters were described using noncompartmental methods. Statistical significance was determined using a two-tailed, unpaired Student's t test with unequal variance. There was no significant difference between AS and SS concentrations at any time points or in the derived PK parameters. (C) The Pearson correlation coefficient for the AUC (h*µg/ml) values derived from multiple GalNAc-siRNAs tested

TABLE 1

Plasma pharmacokinetic parameters from subcutaneous dosing of multiple siRNAs to male (M) and female (F) rats and monkeys

		Plasma Pharmacokinetic Properties after Subcutaneous Administration to Monkeys									
		C_{max}		AUC_{last}		T_{max}		$t_{1/2}$		Dose at C_{max}	
siRNA	Dose	M	F	M	F	M	F	M	F	M	F
	mg/kg	*ng/ml*		*h*ng/ml*				*h*		*%*	
1	0.3	40.6	57.6	233	266	1	2	8.79	ND	0.159	0.225
	3	634	598	4700	3310	2	2	2.78	2.11	0.248	0.234
	10	2530	2860	15,700	16,600	2	2	1.96	5.84	0.297	0.335
2	1	89.3	173	279	465	1	1	ND	ND	0.105	0.203
	5	857	702	4820	4260	2	2	ND	ND	0.201	0.165
	10	2060	2030	11,300	10,600	1	2	3.36	ND	0.242	0.238
15	0.3	43.8	30.6	189	162	1	1	2.38	2.84	0.171	0.119
	1	96.2	112	695	686	1	1	3.24	3.37	0.113	0.131
	3	358	425	2190	2680	2	2	2.79	2.5	0.140	0.166
3	1	72.9	64	112	87	2	2	ND	ND	0.0854	0.075
	5	386	281	1930	1690	2	2	ND	ND	0.0904	0.0658
	25	2560	2130	19,700	12,000	2	1	3.79	6.13	0.120	0.0998
4	0.3	82.1	86.8	198	204	1	1	ND	ND	0.321	0.339
	1	245	311	843	949	1	0.5	2.55	1.52	0.287	0.364
	5	1140	1250	5610	5850	1	1	3.04	1.81	0.268	0.293
	20	6770	4480	44,000	38,000	2	4	8.49	ND	0.396	0.263
5	0.1	13.8	13.2	168	22.5	4	1	ND	ND	0.161	0.155
	1	181	129	12,200	1140	2	2	ND	9.94	0.212	0.151
	5	1160	985	5590	4240	2	2	ND	ND	0.272	0.231
	10	1570	2250	12,100	10,700	2	2	3.58	ND	0.184	0.263
6	0.3	42.2	37.6	119	127	0.5	2	6.22	ND	0.165	0.147
	1	90.6	99.7	586	662	4	4	ND	ND	0.106	0.117
	3	549	299	3140	1600	4	2	ND	ND	0.214	0.117
	30	7760	6920	63,100	66,100	2	4	2.7	ND	0.303	0.270
siRNA	Dose	Plasma Pharmacokinetic Properties after Subcutaneous Administration to Rats									
		C_{max}		AUC_{last}		T_{max}		$t_{1/2}$		Dose at C_{max}	
		M	F	M	F	M	F	M	F	M	F
	mg/kg	*ng/ml*		*h*ng/ml*				*h*		*%*	
1	0.3	34.7	29.1	39.6	16.8	1	1	ND	ND	0.453	0.381
	1	90.5	92.4	174	171	1	1	ND	ND	0.355	0.363
	3	290	301	494	479	1	1	ND	ND	0.379	0.395
	10	1430	1060	3740	2120	1	1	ND	1.38	0.561	0.415
2	1	98	112	141	158	0.25	0.25	ND	2.54	0.384	0.44
	1	102	113	254	164	2	1	ND	ND	0.401	0.442
	5	466	386	1400	1110	0.5	0.25	3.14	1.66	0.365	0.303
	5	568	455	1580	1240	2	1	ND	ND	0.445	0.357
	10	976	1170	2390	2980	0.25	2	3.31	ND	0.383	0.458
	10	1120	1550	4150	3820	2	2	6.33	ND	0.441	0.607
3	2.5	230	285	320	371	0.5	0.5	ND	ND	0.36	0.447
	5	514	639	934	762	1	0.5	ND	ND	0.403	0.502
	25	4450	3980	10,300	7080	1	1	1.43	ND	0.698	0.625
4	0.3	71.4	93.9	101	111	0.5	0.5	ND	ND	0.933	1.23
	1	312	207	415	262	0.5	0.5	0.969	ND	1.22	0.814
	5	943	943	1840	2020	0.25	0.5	0.931	0.83	0.739	0.741
	20	4130	4990	16,200	10,600	0.5	1	ND	1.02	0.809	0.981
5	0.1	21.7	22	15	14.2	0.5	0.5	ND	0.987	0.849	0.865
	1	271	335	381	498	0.5	0.5	1.03	ND	1.06	1.32
	5	1010	874	1820	2020	0.5	1	1.05	1.11	0.793	0.687
	10	2200	2430	4770	4620	1	0.5	0.914	ND	0.864	0.955

F, female; M, male; ND, not determined.

volume), Table 1. There are differences between the plasma PK profile when comparing intravenous and subcutaneous dosing (Fig. 2G), which leads to higher initial plasma concentrations after intravenous dosing. These circulating concentrations can lead to saturation of ASGPR-mediated uptake clearance, thereby complicating the interpretation of systemic bioavailability.

Designing experiments to determine the absolute systemic bioavailability is complicated by a desire to use a low enough dose to avoid

at increasing dose levels in rat (*x*-axis) and monkey (*y*-axis). (D) The Pearson correlation coefficient for the AUC (h*μg/ml) values derived from multiple GalNAc-siRNAs tested at increasing dose levels in monkey (*x*-axis) and human (*y*-axis). (E) The AUC (h*μg/ml) values derived for increasing subcutaneous dose levels of seven GalNAc-siRNA in human, and (F) the same data derived in monkey. In these panels, siRNA15 is depicted by the blue circle, siRNA2 by the red square, siRNA21 by the green upward triangle, siRNA5 by the purple downward triangle, siRNA6 by the orange diamond, siRNA7 by the black circle, and siRNA13 by the brown square. (G) The concentration-time profile for siRNA1 (blue circle; closed is after intravenous administration of 10 mg/kg, and open is after subcutaneous administration of 10 mg/kg), siRNA2 (red square; closed is after intravenous administration of 10 mg/kg, and open is after subcutaneous administration of 10 mg/kg), and siRNA5 (green triangle; closed is after intravenous administration of 5 mg/kg, and open is after subcutaneous administration of 5 mg/kg). The table shows the derived PK parameters and the estimated % bioavailability (%F) from these studies.

ASGPR saturation while still dosing high enough to enable adequate plasma exposure to accurately characterize the AUC. Because of rapid ASGPR-mediated distribution into the liver, the plasma exposure of GalNAc-conjugated siRNA is limited and thus requires relatively high dose levels to ensure detection long enough to characterize plasma PK parameters. When high doses are administered via intravenous bolus injection, the systemic exposure reaches levels that saturate the ASGPR uptake capacity for a period of time after injection, which subsequently reduces the distribution into liver in the intravenous group. Saturation is less impactful in subcutaneous doses, in which systemic absorption from the injection site is gradual, resulting in relatively low plasma concentrations that do not saturate ASGPR uptake. To compute the true absolute bioavailability, the potential for ASGPR saturation can be reduced by incorporating 1-hour infusions in place of intravenous bolus dosing to generate conditions similar to those observed after subcutaneous doses at pharmacologically relevant doses (McDougall et al., 2019). Optimal dose levels and sampling time points for an intravenous infusion were identified using plasma PK modeling, striking a balance between replicating the subcutaneous clearance conditions with a systemic dose while generating plasma PK profiles that can accurately characterize the AUC. The systemic bioavailability of subcutaneous GalNAc-conjugated siRNA determined under this new paradigm, although variable, is much higher (on average near 100%) than when intravenous bolus dosing is used as the reference and, importantly, is better aligned with estimated liver levels after subcutaneous dosing (Table 2). The variability in the measured absolute bioavailability underscores the complexity of attempting to use plasma PK to describe absolute systemic bioavailability, particularly in the presence of active liver uptake.

Biodistribution. Given that GalNAc-siRNA is designed to target liver-derived diseases and thus liver is the target organ, nonclinical studies have aimed to thoroughly characterize the pharmacokinetic parameters in liver. This has been accomplished through liver sampling during rat and monkey PK/PD studies for a large number of GalNAc-conjugated siRNAs. Upon absorption into systemic circulation after a subcutaneous administration, GalNAc-conjugated siRNAs are quickly and predominantly taken up by liver, with liver C_{max} observed around 4–8 hours in rats and 8–24 hours in monkeys. There are no significant sex-dependent differences in exposure, and the liver PK is reproducible across conjugates and linear with dose level up to 10 mg/kg (Fig. 3, A–J). The liver exposure significantly exceeds the plasma exposure in all cases, despite some variability in absolute amounts, which suggests that there may be some sequence dependence on either the extent of liver uptake or intracellular metabolic stability. The overall liver-to-plasma ratio, calculated by division of measured AUC values, is high, with average ratios of 6,300 in monkey and 5,500 in rat (Table 3). In general, after subcutaneous administration of pharmacological dose levels, up to 63% of the dose is recovered in liver of rats, and up to 87% of the dose is recovered in the liver of monkeys. The percentage of dose recovered in liver decreases with increase in subcutaneous dose level. The percentage of total dose in liver is also lower after intravenous dosing at the same dose level used in subcutaneous dosing: up to 17% of dose in rat and monkeys.

TABLE 2

Estimated %F from traditional intravenous bolus or 1-hour infusions compared with subcutaneous administration

	DN AUC_{last} Subcutaneous/DN AUC_{last} Intravenous		
siRNA	Bolus or Infusion	Rat	Monkey
siRNA1	Bolus	15	ND
siRNA2	Bolus	24	37
	1-h infusion	225	ND
siRNA3	Bolus	25	23
siRNA4	Bolus	23	31
siRNA5	Bolus	31	50
siRNA6	Bolus	13	14
	1-h infusion	104	ND
siRNA 9	1-h infusion	148	115
siRNA18	1-h infusion	32	79
siRNA22	Bolus	37	51

DN, dose normalized; ND, not determined.

The liver half-life can be used, along with RISC loading data, to describe the pharmacodynamics of GalNAc-conjugated siRNA [characterizing the key PK/PD relationship in target tissue (liver)] and is therefore an important parameter to characterize during nonclinical studies. The liver half-lives observed for first-generation conjugates (STC) ranged between 4 and 10 hours in rats and monkeys, respectively [example using the same sequence revusiran (STC) and vutrisiran (advance ESC) is provided in Fig. 10B]. Liver half-lives observed with ESC, Advanced ESC, and ESC+ tend to overlap and range between 50 and 230 hours in rats and 146 and 840 hours in monkeys. The longer liver half-life in monkeys compared with rodents can be recovered by scaling clearance with bodyweight and an exponent typically less than 1. The liver half-lives for a number of ESC molecules have also been evaluated in mice and were determined to be consistent with those derived from rats (between 37.0 and 175 hours).

To evaluate renal distribution of GalNAc-conjugated siRNAs, several studies also characterized the PK for GalNAc-siRNA in kidney. Studies in rats with siRNA2 or siRNA4 were designed to compare liver and kidney concentrations over a wide dose range. These studies showed that, at pharmacologically relevant dose levels, there is very high distribution to the liver, with a smaller fraction (up to 25-fold lower) distributed to the kidney. In rat, siRNA2 liver-to-kidney ratios were 25, 14, 4.5, 5.0, 1.5, and 1.5 at 1, 5, 10, 30, 100, and 300 mg/kg, respectively. A similar observation was made for siRNA4, for which liver-to-kidney ratios were 8.2, 7.8, 3.1, 3.3, 1.3, and 0.85 after the same subcutaneous dose levels as siRNA2. The overall distribution between liver and kidney was dose-dependent, with the ratio decreasing at supratherapeutic doses, likely due to ASGPR saturation. Similar studies in monkey were consistent with studies in rat in which the liver-to-kidney ratio decreased with increasing dose level; for example, after subcutaneous dosing of siRNA8, the ratio dropped from 57 at 30 mg/kg to 24 at 150 mg/kg. Similar observations were made for two other GalNAc-siRNAs for which terminal kidney levels were measured at multiple dose levels; furthermore, these studies demonstrate that the ratio between liver and kidney in monkey is higher than that observed in rat.

A series of studies were conducted to characterize the mass balance, tissue distribution, excretory, and metabolite profiles in rat using radiolabeled GalNAc-conjugated siRNA. because of the large molecular weight, and to balance the radioactive signal with the pharmacological dose level, tritium was selected as the radiolabel to support these nonclinical investigations. In the three GalNAc-conjugated siRNAs evaluated, the radiolabel was placed on an adenosine nucleotide centrally located in the antisense strand. Total radioactivity recovered in urine and feces during the studies was between 75% and 90%. siRNA20 is an STC molecule and thus has lower stability than siRNA2 and siRNA6, which are ESC and Advanced ESC molecules, respectively. The QWBA data demonstrate that the overall distribution profiles between the three GalNAc-conjugated siRNAs evaluated are consistent with primary distribution to liver followed by much lower distribution to kidney and extrahepatic tissues (Fig. 4). There was less than 10% of the total dose recovered in the injection site by 24 hours, which was consistent across studies and consistent with a study in rat using nonradiolabeled siRNA2 in which 6% of the dose was recovered in tissue

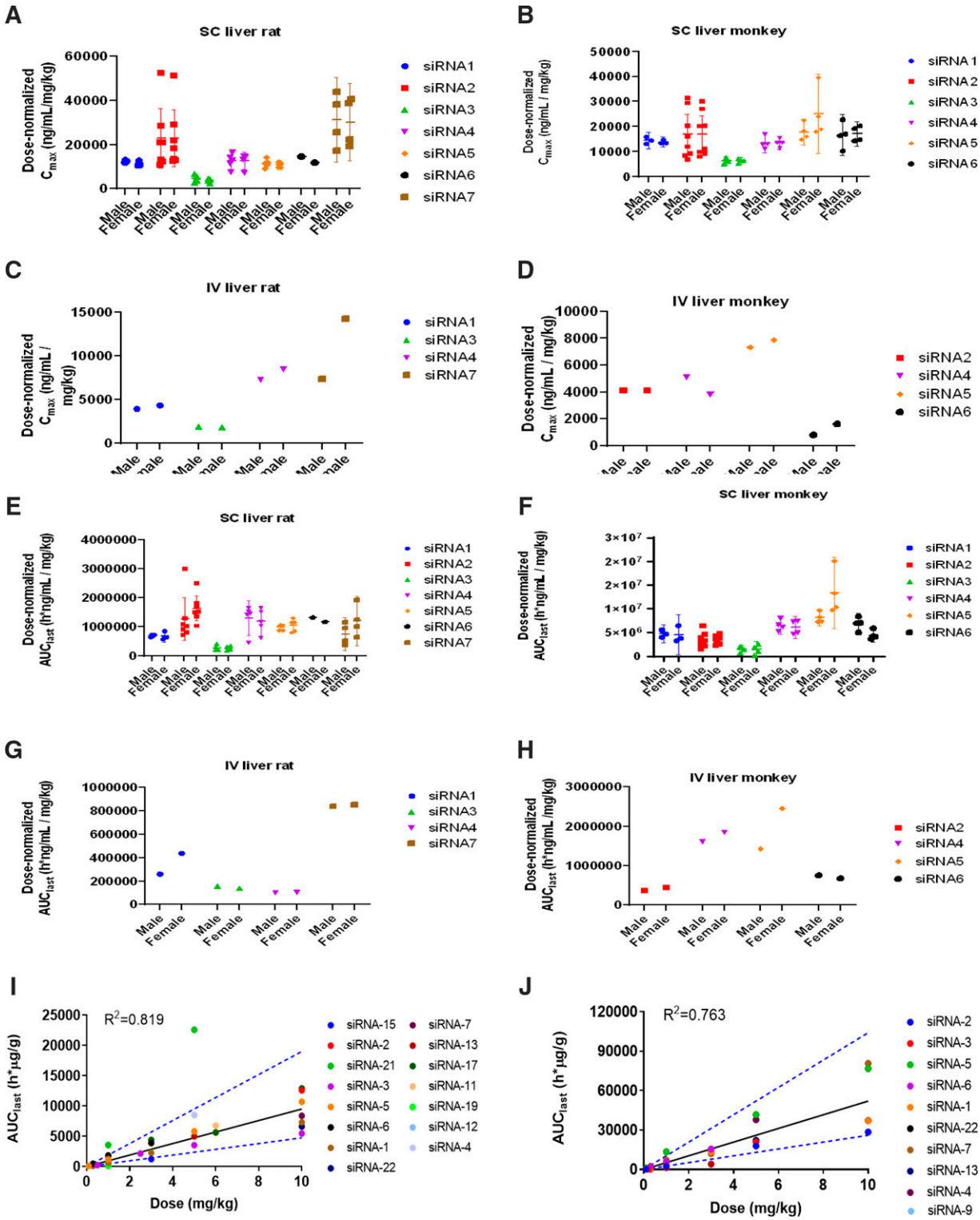

Fig. 3. Dose-normalized C_{max} (A–D) and AUC (E–H) values in male and female livers after subcutaneous administration to rat (A and E), subcutaneous administration to monkey (B and F), intravenous administration to rat (C and G), and intravenous administration to monkey (D and H). The horizontal line represents the median data point, and the vertical lines represent the 90% confidence intervals in (A), (B), (E), and (F), where multiple dose levels were evaluated after subcutaneous administration. For intravenous dosing, only a single dose level was administered, and the data points represent the composite mean value for $n = 3$ rats or monkeys. In these panels, siRNA1 is represented by a blue circle, siRNA2 by a red triangle, siRNA3 by a green upward triangle, siRNA4 by a purple downward triangle, siRNA5 by an orange diamond, siRNA6 by a black square, and siRNA7 by a brown square. Statistical significance between PK parameters across GalNAc-siRNA between males and females was evaluated using a two-tailed, unpaired Student's *t* test with unequal variance, and there were no statistically significant findings. (I and J) The AUC (h*µg/g) determined in liver following increasing subcutaneous dose levels of siRNA1 through siRNA22 (depicted with varying color circles) in rat (I) and monkey (J). The black line represents the mean linear regression for the data set, whereas the blue lines represent the slopes between 2- and 0.5-fold of the mean.

TABLE 3

Representative ratio of liver/plasma after subcutaneous administration decreases with increasing dose in rat and monkey

siRNA	Dose		AUC_{last} Liver/AUC_{last} Plasma	
	Rat	Monkey	Rat	Monkey
	mg/kg			
siRNA1	0.3	0.3	4905	6110
	1	ND	3967	ND
	3	3	4482	2455
	10	10	1955	4123
siRNA2	1	1	3206	7758
	5	5	4125	3473
	10	10	2215	4142
siRNA3	2.5	1	3233	12,558
	5	5	1648	4729
	25	25	ND	2634
siRNA4	0.3	0.3	14,476	12,169
	1	1	19,816	11,927
	5	5	16,621	6628
	20	20	ND	2382
siRNA5	0.1	0.1	6887	5749
	1	1	2776	ND
	5	5	2899	7337
	10	10	1848	6063
siRNA6	ND	0.3	ND	21,098
	ND	1	ND	11,927
	ND	3	ND	6628
	ND	30	ND	2382

ND, not determined

removed from the injection site area at 6 and 24 hours post–subcutaneous dosing of 5 mg/kg per rat.

Limited microautoradiography (MARG) data in the liver demonstrates that, after a dose of 3 mg/kg, the majority of radioactivity is located in zone 1 (periportal), with moderate levels present in zones 2 (intermediary) and 3 (centrilobular). There is also radioactivity observed at the canalicular membrane and in the bile, suggestive of exocytosis into bile (Fig. 4, B and C). Both of these observations are consistent with findings from histopathology examinations in liver samples from rats and monkeys dosed with increasing dose levels of GalNAc-conjugated siRNA (data not shown).

The blood cell partitioning was determined during the radiolabeled excretion studies and was ≤ 1 for the three molecules tested, indicating that GalNAc-siRNAs do not preferentially distribute into blood cells.

Metabolism. To investigate the metabolic stability of the GalNAc ligand in more detail, a series of in vitro and in vivo studies were conducted. An in vitro incubation with hepatocytes from rat, monkey, and human indicated faster cleavage and amidase activity in rat, whereas the rates observed between monkey and human were similar (Table 4). Incubations of 160 μg/ml siRNA2 with *β-N*-acetylglucosaminidase showed near-complete loss of GalNAc moieties by 2 hours (9% remaining), whereas minimal loss was observed in serum incubations from rat, monkey, and human by up to 24 hours (<25%). Further in vivo plasma data show minimal loss of GalNAc after subcutaneous administration (91% of intact sense strand for siRNA17, 97% of intact sense strand for siRNA16). In contrast, studies evaluating the pH dependence of GalNAc cleavage demonstrate that higher GalNAc loss is observed under acidic pH conditions; 95% of intact GalNAc remained after a 4-hour incubation with mouse liver lysosomal lysate at pH 7 versus 32% at pH 5. Metabolite profiling of siRNA6 in liver samples from rat and monkey indicate that the sense strand is metabolized by sequential loss of GalNAc moieties followed by cleavage of amide bonds at positions 1 (linker 1) through 3 (linker 3); refer to Fig. 1A. In rat, 79% of the sense strand of siRNA6 in hepatocytes lost all three GalNAc moieties at the first time point (<15 minutes after dosing), and importantly, no sense strand with all three GalNAc moieties was observed. After 7 hours, 57% of the sense strand shows varying degrees of sequential linker metabolism (Supplemental Fig. 2). In monkey liver, 87% of the sense strand of siRNA6 was recovered lacking all three GalNAc moieties at 8 hours postdose. Similar to the in vitro incubation, the loss of amide bonds occurred more slowly in monkey than in rat (Supplemental Fig. 2). Taken together, these results demonstrate that, upon subcutaneous administration of GalNAc-conjugated siRNAs, the GalNAc moieties are quickly cleaved by *β-N*-acetylglucosaminidase during endo/lysosomal trafficking, and the linker structure is further metabolized by amidases in hepatocytes.

Duplex siRNA undergoes metabolism through exo- and endonucleases ubiquitously distributed in plasma and tissues rather than through cytochromes P450 (Ramsden et al., 2019). Exonucleases work on the end of the strand, resulting in release of mononucleotides, whereas endonucleases cleave internally and result in strands of varying lengths (Fig. 1B). The metabolic scheme is presented in Fig. 1. Metabolite profiling of plasma, urine, feces, and bile from radiolabeled mass balance studies demonstrates that siRNA6 was cleared in rats via a combination of metabolism and renal and biliary clearance of parent drug. In plasma, unchanged siRNA6 accounted for approximately 75% of the total radioactivity exposure through 96 hours (AUC0–96) postdose. 3′N-1 contributed 6.86% of the of the total radioactivity exposure. Radioprofiles of urine samples showed that unchanged siRNA6 accounted for 3.71% and 5.75% of the dose from intact and BDC rats, respectively. 3′N-1 accounted for 0.213% of the dose in urine from intact rats. Approximately 22.9% and 14.0% of the dose in intact and BDC rats, respectively, eluted at the void volume. Efforts to identify the components of this peak were unsuccessful (M1), but the peak likely comprises multiple dimers or shortmers containing the radiolabel and not a single metabolite. Approximately 9% of the dose was recovered as unchanged siRNA6 in bile. 3′N-1 accounted for approximately 3% of the dose in bile. All the radioactivity recovered in feces was associated with unknown components. No unchanged siRNA6 was recovered in feces from intact rats. [^{3}H]siRNA6 was metabolized in rats after subcutaneous administration via hydrolysis. Most of the [^{3}H]siRNA20-derived radioactivity was excreted after subcutaneous administration over 168 hours after dosing (intact rats), primarily in urine. After subcutaneous administration to intact rats, means of 67% and 7% of the administered radioactivity were excreted in urine and feces, respectively, by 1344 hours postdose. In BDC rats after subcutaneous dosing, means of 57.0%, 16.6%, and 1.91% of the administered radioactivity were excreted in urine, bile, and feces, respectively, by 168 hours postdose. A large amount of radioactivity was eliminated in urine after subcutaneous dosing, indicating that renal excretion was a major route of elimination of [^{3}H]siRNA20-derived radioactivity. The analysis of urine and bile samples for radioactivity before and after drying indicated the fraction of radioactivity in the form of tritiated water generally increased over time for urine and bile. The mean overall recoveries of radioactivity after subcutaneous dosing to intact and BDC rats were 82.8% and 89.2%, respectively. It is possible that the lower recovery of radioactivity was due to expiry of tritiated water. Radioprofiles of urine samples showed that unchanged siRNA20 accounted for 1.67% and 0.805% of the dose from intact and BDC rats, respectively. 3′N-1 accounted for 0.555% and 2.84% of the dose in urine from intact and BDC rats, respectively. Approximately 56% and 46% of the dose in intact and BDC rats, respectively, eluted at the void volume. Efforts to identify the components of early eluting peaks, M1/M2, were unsuccessful, but the peaks likely comprised multiple dimers or shortmers containing the radiolabel (not a single metabolite) and also a considerable portion of tritiated water based on the urine-drying experiment. In bile, approximately

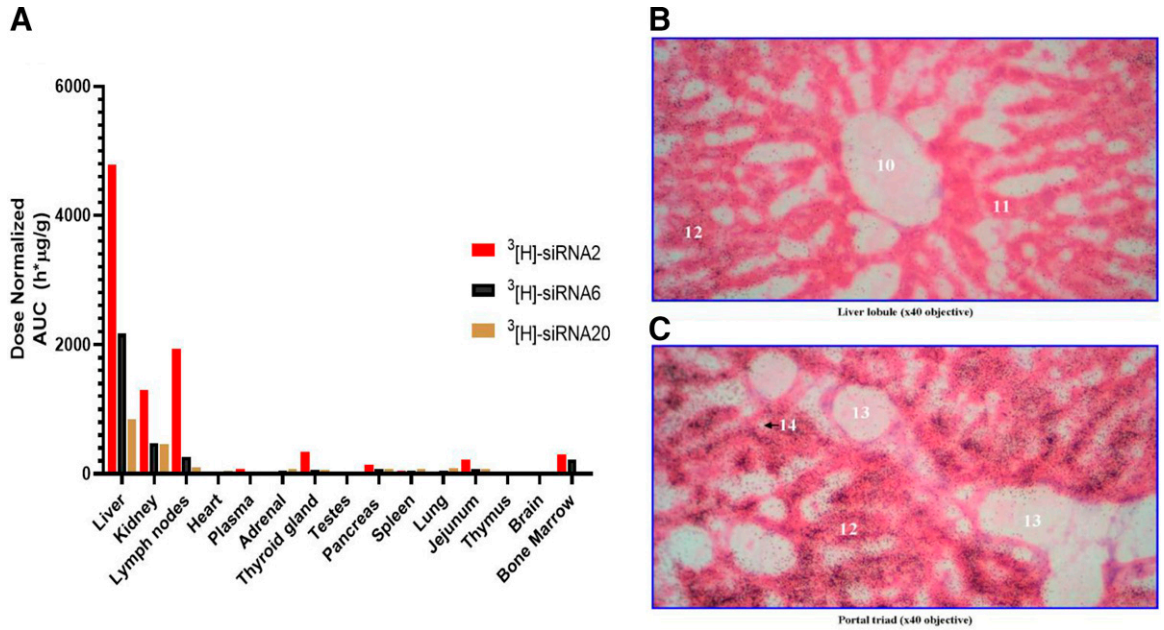

Fig. 4. Tissue distribution profile in rats after subcutaneous administration of radiolabeled siRNA2 (3 mg/kg), siRNA5 (3 mg/kg), and siRNA20 (10 mg/kg) to rats based on the estimated dose-normalized AUC (h*µg/g) (A) from the QWBA analysis. The QWBA data represents the composite value of $n = 3$ animals per time point. (B and C) The microautoradiography results after 3 mg/kg administration of siRNA5 to rats. In these pictures, the annotations of 10, 11, 13, and 14 represent the central vein, the centrilobular region, the periportal region, the portal vein, and the bile duct, respectively.

1% of the dose was recovered as unchanged siRNA20. 3′N-1 was recovered in bile and accounted for approximately 1% of the dose. [^{3}H]siRNA20 was metabolized in rats after subcutaneous administration via hydrolysis. Four metabolites were tentatively identified in addition to 3′N-1 and unchanged siRNA20. Metabolite profiling and identification results indicate that siRNA20 was primarily cleared in rats via metabolism. Loss of a single nucleotide from the 3′ end of the antisense strand, annotated as 3′ ′N-1(AS), is an often-observed metabolite in liver samples confirmed by mass spectrometry analysis (Fig. 5). The 3′ N-1(AS) metabolite is typically as potent as the parent molecule (Table 5). Formation of this active metabolite in monkey liver can differ across GalNAc conjugates targeting different mRNAs (Fig. 5). Additional truncation of metabolites can range in activity compared with the full-length siRNA with 5′ nucleotide loss generally rendering inactive metabolites (Table 5). Limited data have been generated confirming that loading efficiency of the active metabolites into RISC is equivalent to the parent compound. The formation of metabolites appears to be conserved across species, enabling extrapolation between in vitro and in vivo data (Supplemental Table 2; Table 4).

Excretion. The mass balance data from radiolabeled ADME studies in rat coupled with metabolite profiling data from plasma, urine, feces, and bile demonstrate that most of the radioactivity was excreted as truncated metabolites in urine, with a small fraction (<25%) representing intact antisense strand. These results are consistent with the urinary excretion data obtained using unlabeled GalNAc-conjugated siRNAs. In bile duct–cannulated rats, the radioactivity is eliminated primarily through truncated metabolites, and full-length antisense to a limited extent. The radioactivity recovered in feces of intact rats was less than the amount of radioactivity excreted in bile of BDC rats, suggesting that some truncated metabolites can undergo enterohepatic reabsorption. Data across five GalNAc-conjugated siRNAs including radiolabeled mass balance studies demonstrate that the extent of biliary clearance of intact siRNA is limited (10%–20%). A caveat when interpreting these data is that biliary excretion was only measured for 1 week in

TABLE 4

In vitro GalNAc and linker metabolism for siRNA8 in cultured hepatocytes

	Total AUC siRNA8 Sense Strand Metabolite Profile		
Analyte	Rat	Monkey	Human
		%	
−3 GalNAc	Not detected	48.7	45.0
−3 GalNAc, −1linker1	Not detected	20.3	27.5
−3 GalNAc, −1linker1, −1linker2	Not detected	5.2	Not detected
−3 GalNAc, −2linker1	Not detected	12.2	14.9
−3 GalNAc, −2linker1, −1linker2	Not detected	3.6	Not detected
−3 GalNAc, −3linker1,	99.5	8.5	11.0
−3 GalNAc, −3linker1, −1linker2	Not detected	1.6	Not detected
Full-length siRNA8	66.6	71.0	74.9
AS(N-1)3′ siRNA8	29.7	21.2	15.9

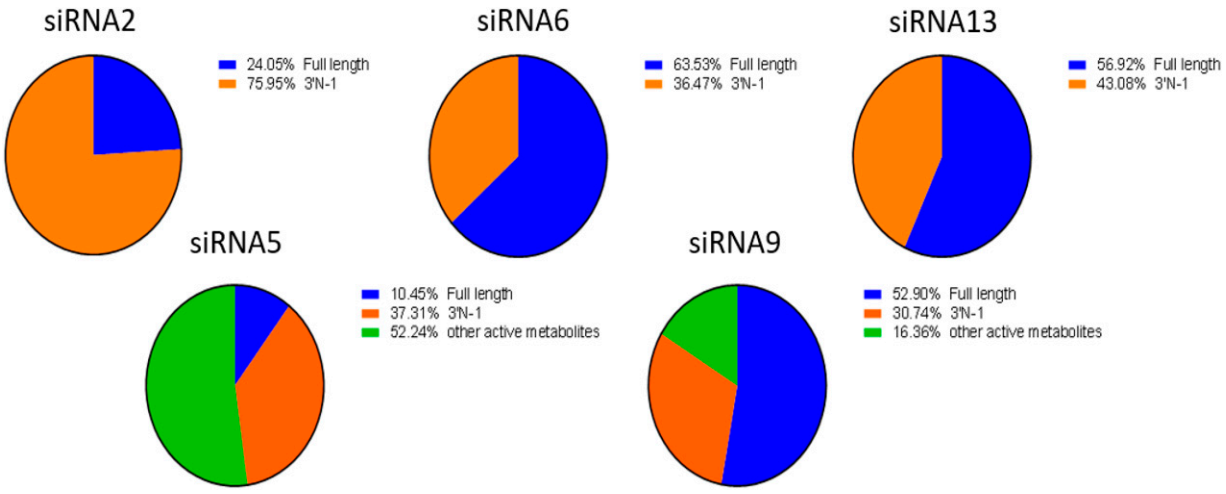

Fig. 5. Metabolite profiles for siRNA2, siRNA5, siRNA6, siRNA9, and siRNA13 in homogenate prepared from monkey livers after subcutaneous dosing. The percentage of full-length (blue) compared with 3′N-1 (orange) and other active metabolites (green) is derived from the AUC profile either as a pool or discrete time point samples. In all cases, authentic standards were used to determine the quantitative levels of full-length or metabolites, and the sum of the individual components was used to derive the percentage of total.

cannulated rats. In addition, depending on where the radiolabel is placed, there can be a classic double peak, suggestive of enterohepatic recirculation (Fig. 6A). Metabolite profiling of samples taken during the double peak reveal that the majority of radioactivity is contained within shortmer metabolites and that no peak corresponding to active metabolites or full-length GalNAc-conjugated siRNA2 is observed (Fig. 6B). PD evaluation in bile duct–cannulated rats shows that there is no impact on PD, suggesting that any excreted full-length siRNA does not undergo hepatobiliary recycling to further contribute to PD (Fig. 7). This is consistent with the GalNAc metabolism data demonstrating that the GalNAc moieties are quickly cleaved under acidic conditions during endocytic trafficking.

Renal excretion of full-length siRNA, as a percentage of total drug administered, has been investigated for multiple GalNAc-conjugated siRNA in nonclinical models including rat and monkey during routine PK studies after subcutaneous administration (Table 6). Across different conjugates designed for various targets, the urinary excretion was less than 25%. This was also the case when these molecules were dosed to humans (Agarwal et al., 2020; Habtemariam et al., 2021).

To investigate whether reduced kidney function may lead to changes in plasma or liver PK, renal excretion, or PD outcomes, the 5/6 nephrectomy model was evaluated. The 5/6 nephrectomy model has been successfully employed to evaluate the impact of chronic renal failure on designated endpoints, including toxicity and PK (Glund et al., 2018; Kujal and Vernerová, 2008; Li et al., 2012; Ozcan et al., 2012; Tapia et al., 2013). This model was successfully qualified in our laboratory, and aggregate analysis of three nephrectomy studies demonstrates no meaningful differences in the plasma and liver PK or PD of GalNAc-conjugated siRNA in rats with and without nephrectomy. Although there was a decrease in urinary excretion of full-length GalNAc-conjugated siRNA in rats with nephrectomy relative to those without nephrectomy, these data confirmed that renal excretion plays a minor role in the overall elimination of RNAi therapeutics. Importantly, moderate to severe renal impairment does not influence the liver concentration and target mRNA reduction (Table 7).

Characterizing the Key PK/PD Relationship in Target Tissue (Liver). The PK/PD relationship of GalNAc-conjugated siRNA is more complex than conventional small molecules, as plasma PK does not correlate directly with the PD effect. First, there is a significant difference between plasma PK T_{max} and the corresponding PD T_{max}. Plasma T_{max} from subcutaneous doses is achieved quickly, between 0.2 and 12 hours, whereas PD T_{max} occurs later, typically at least 3 days after dosing in mice, 1 week after dosing in rat, and 2 weeks after dosing in monkey (Fig. 9, representative data; additional examples not shown). Liver T_{max} occurs later than plasma T_{max}, typically between 8 and 24 hours postdose in all species, but still proceeds PD T_{max} significantly. Only the kinetics of siRNA in RISC, with a T_{max} coincidental with maximal PD response, shows a direct relationship between PK T_{max} and PD T_{max} (Fig. 8, C and D). A second complexity results from a disconnect between the plasma PK half-life, less than 8 hours in all species (Table 1), and the prolonged duration of the PD remaining for weeks in rodents and up to several months in monkeys and humans. PD effect profiles correspond much more directly with the liver half-life and siRNA exposure in RISC than the plasma half-life (Fig. 8), and the metabolic stability of siRNA in liver has been key to realizing long-term stable target reduction with infrequent dosing.

TABLE 5

Pharmacological activity assessment for siRNA2 metabolites (transfected) in plated HEP3B

Designation (AS)	Target mRNA Baseline Remaining
	%
Parent	16.4
3′N-1	10.3
3′N-2	11.4
3′N-3	13.5
3′N-4	15.9
3′N-5	12.2
3′N-6	47.7
3′N-7	81.1
3′N-8	95.7
5′N-1	78.6
5′N-2	20.7
5′N-3	89.0
5′N-4	78.5
5′N-5	95.2
5′N-6	100
5′N-7	100
5′N-8	100

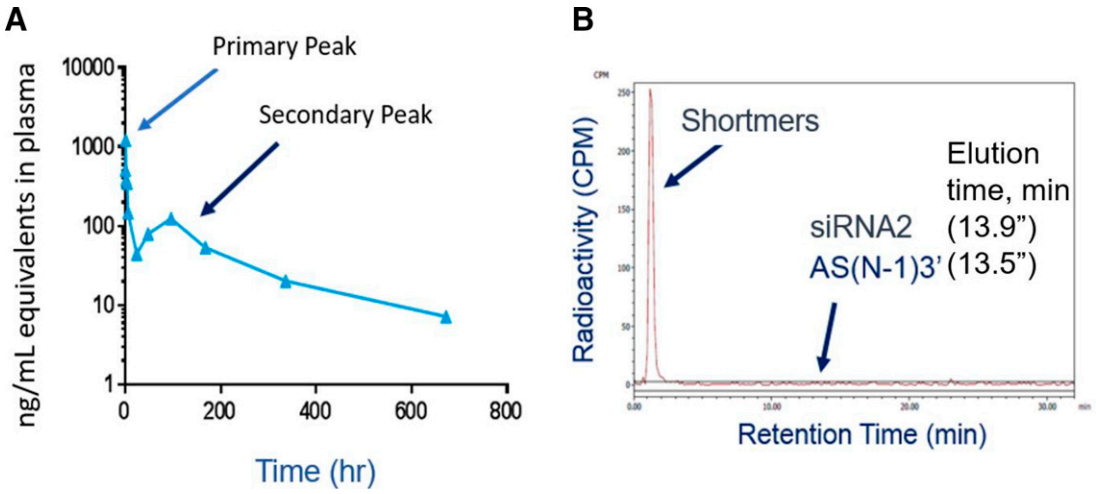

Fig. 6. After subcutaneous administration of [^{3}H]siRNA2 in rats, a secondary peak of radioactivity was observed starting around 120 hours postdosing. (A) The primary and secondary radioactivity peaks, which already account for the release of tritiated water via deduction. Evaluation of the radiochromatogram from plasma samples taken at the maximum of this secondary peak (B) demonstrates that all of the radioactivity elutes early, where shortmer (>3 but <7 oligonucleotides), dimer (2 oligonucleotides), or monomers (single nucleotides and/or nucleosides) elute. There were no peaks observed at the elution times for siRNA2 (13.9 minutes) or the active metabolite AS(N-1)3′ (13.5 minutes).

When the same GalNAc-siRNA was active across multiple species, the onset of activity in rodents occurs earlier than in monkeys and humans, and the duration of effect was shorter. Similarly, the duration of pharmacological activity was shorter in monkey than in human (Fig. 9). The plasma, liver and RISC PK can be scaled across species allometrically, with higher clearance rates observed in mice/rats compared with monkeys and humans. An example of this is provided for revusiran, an STC molecule, and vutrisiran, an advanced ESC molecule (Zimmermann et al., 2017; Habtemariam et al., 2021) (Fig. 10). Both of these are GalNAc-conjugated siRNAs and contain the same sequence targeting human transthyretin mRNA. In humans, revusiran required a 5-day daily loading dose (500 mg) followed by weekly dosing, whereas vutrisiran can be dosed in humans at 25 mg every 3 months and maintain similar reduction of circulating transthyretin (TTR) levels throughout. As depicted in Fig. 10, the impact of improved metabolic stability of vutrisiran results in increased liver exposure (Fig. 10A), and half-life (Fig. 10B) in monkey, which translates to durable pharmacodynamics after reduced dose levels and frequency (Fig. 10C). This is reproduced during human clinical trials in which, once dosing of revusiran is stopped, the TTR levels swiftly recovered, whereas the TTR reductions were maintained for several months after single doses of vutrisiran (Fig. 10D) (Habtemariam et al., 2021). In vitro data, generated in serum and S9 from rat, monkey, and human, also showed a trend for lower metabolic stability with revusiran compared with vutrisiran, although the data were not quantitative with respect to predicting half-life.

The direct PD driver of GalNAc-conjugated siRNA drugs is the amount of siRNA (antisense strand) loaded in RISC, with the observed PD effect (as measured by reduction of target protein in plasma) corresponding directly with the concentration of RISC-loaded siRNA (Fig. 8, C and D). RISC T_{max} typically ranges between 3 and 7 days in both rats and monkeys. The RISC C_{max} is significantly lower than that in liver, often by 1000-fold or more (Castellanos-Rizaldos et al., 2020).

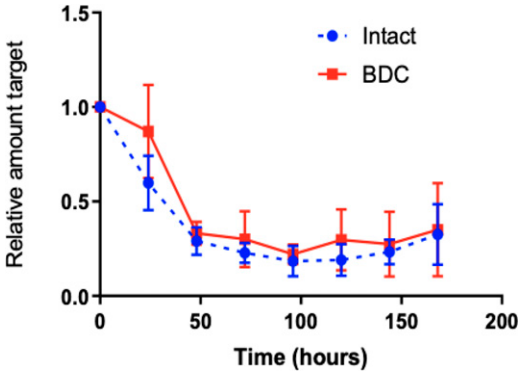

Fig. 7. Pharmacodynamics were measured after subcutaneous administration of 1 mg/kg siRNA11 to intact female rats (blue) or bile duct–cannulated female rats (red) using a commercially available ELISA kit toward the target protein in serum. The *y*-axis is the relative amount of target remaining, and the *x*-axis is the time point in hours. Each point represents the mean of three animals per time point, with the bars representing the S.D. A two-tailed, unpaired Student's *t* test with unequal variance was used to evaluate whether there were any statistical differences between the intact and BDC rats at each time point. There were no statistically significant differences between the groups observed.

Discussion

For the development of RNAi therapeutics, understanding the translation of nonclinical PK/PD and ADME properties across compounds and species enables prediction and subsequent understanding of these attributes in humans. The majority of the siRNAs currently in clinical development are conjugated to GalNAc ligands for targeted delivery to the liver. Here, we describe the development of the tools and the design of studies to 1) investigate the similarity of absorption, biodistribution, metabolism, and excretion properties across compounds and species; 2) characterize metabolic stability and its impact on dosing regimen; and 3) elucidate siRNA exposures in liver and RISC as direct drivers of PD, which are used to project human efficacious dose through allometric scaling. These nonclinical evaluations have assisted the optimization of chemical modifications and delivery systems, ultimately resulting in the approval of four RNAi therapeutics and proof of clinical efficacy for many more currently in late-stage clinical development (Debacker et al., 2020).

Several recent publications have highlighted the bioanalytical approaches used to quantify levels of GalNAc-conjugated siRNA from various biologic matrices (Li et al., 2019; Liu et al., 2019; Castellanos-Rizaldos et al., 2020). Given the instability observed for single strands under in vitro assay conditions and in vivo matrices employed during

TABLE 6

Cross-species renal excretion profiles as a percentage of the total dose

Species	Lumasiran	Givosiran	Vutrisiran
		%	
Rat	9	11	9
Monkey	15–25	19	11–24
Human	8–25	3–17	10–25

nonclinical evaluations, measuring the antisense strand alone can be taken as reflective of the duplex, eliminating the need to characterize both the sense and antisense strand and improving throughput.

To characterize the ADME properties for GalNAc-conjugated siRNA, many nonclinical studies in rats and monkeys have been conducted across current chemistry platforms (ESC, Advanced ESC, and ESC+) on more than 22 GalNAc-conjugated siRNAs containing various sequences and targeting different proteins. The aggregate analysis of these results demonstrates that, at clinically relevant dose levels, there are no sex-dependent differences in plasma or liver PK parameters, and exposures increase in a dose-proportional manner. Furthermore, across various conjugates, the overall dose-normalized exposures are primarily within 2-fold of the mean for plasma, liver, and RISC in rat and monkeys, resulting in highly predictable and extrapolatable plasma and liver PK properties. This enables prediction of expected plasma, liver, and RISC-loaded concentrations for different siRNA molecules while designing toxicology and first-in-human studies. Additionally, the plasma exposure in humans can be predicted from data generated in rats and monkeys, providing confidence in predictions made for human liver PK through allometric scaling from nonclinical models.

The assessment of absolute systemic bioavailability is complicated by the rapid distribution into liver, resulting in low apparent plasma concentrations after subcutaneous doses that are not reflective of overall absorption coupled with saturation of liver uptake with intravenous bolus dosing. Therefore, traditional bioavailability studies relying on intravenous bolus administration at relatively high doses underestimate the bioavailability of subcutaneously administered GalNAc-conjugated siRNA. When evaluating the liver levels at C_{max} as a percentage of the total dose, it becomes clear that much greater levels of GalNAc-conjugated siRNA are absorbed after subcutaneous administration than the measured bioavailability values would suggest. To derive a true bioavailability estimate, studies were designed with optimized infusion time to limit ASGPR saturation while still enabling adequate plasma exposure to characterize the AUC, and multiple recent studies conducted with this new paradigm suggest near-complete bioavailability of GalNAc-conjugated siRNA after subcutaneous administration. The large variability in these infusion experiments, however, suggests that the plasma PK-based method is not a reliable approach to assess the true bioavailability of GalNAc-conjugated siRNA.

Radiolabeled ADME studies conducted in rats have served as a surrogate to conducting these studies in humans. This is primarily driven by the knowledge gained from studies with cold (unlabeled) compounds, which demonstrate cross-species translatability, and the prolonged radioactive exposure in liver that makes human mass balance studies unethical. The distribution pattern for GalNAc conjugates in QWBA studies shows that the majority of radiolabeled GalNAc-conjugated siRNA is observed in the liver, with lower levels in extrahepatic tissues, including kidney, lymph nodes, adrenal gland, pancreas, jejunum, and bone marrow. There was no radioactivity observed in the brain and negligible levels in the heart, largely since ASGPR expression has been shown to be primarily enriched in the liver (Carito et al., 2016). Data presented in Brown et al. (2020) demonstrate that GalNAc-conjugated siRNAs localize in acidic vesicular compartments (likely late endosomes and lysosomes). Radiolabeled ADME studies coupled with MARG data reveal dose dependence in the pattern of distribution within hepatocytes, with higher dose levels achieving more uniform distribution across zones, whereas with lower dose levels (i.e., 3 mg/kg), higher distribution is observed in zone 1 and moderate levels in zones 2 and 3. MARG analysis of siRNA6 also confirmed localization at the bile duct, which is consistent with release into bile through exocytosis of lysosomal content. This result is also consistent with histopathology examinations from rat and monkey liver samples. Negligible levels are observed in cardiac tissue, which taken together with the large molecular size, lack of the human Ether-a-go-go Related Gene (hERG) channel blockade, and no evidence of QT interval prolongation in clinical studies obviates the need to conduct dedicated QT studies in the clinic. Furthermore, upon subcutaneous administration, limited amounts (<10%) are retained at the injection site or in the lymphatic system, limiting the potential for delayed high concentrations released into systemic circulation.

Plasma protein binding has been extensively covered in prior publications using an EMSA method (Rocca et al., 2019). The data demonstrate that plasma protein binding appears to be >85% at clinically relevant concentration levels but is conserved across species, does not limit active ASGPR-mediated uptake (Agarwal et al., 2021), and is saturable at toxicological dose levels (>100 mg/kg) (Rocca et al., 2019). This results in higher "free" GalNAc-conjugated siRNA in the good laboratory practice (GLP) toxicology studies (fraction unbound ~50%) than is observed in the clinical dose range (1%–20% fraction unbound). Therefore, safety margins in nonclinical species based on total siRNA concentrations likely include a conservative estimate. Furthermore, studies using protein pull-down approaches have determined that GalNAc-siRNA does not bind to albumin but does bind to multiple other proteins present in plasma (Agarwal et al., 2021).

TABLE 7

Summary of PK/PD and urinary excretion in rats with and without 5/6 nephrectomy

		Plasma		Liver			
siRNA	Condition	C_{max}	AUC_{last}	C_{max}	AUC_{last}	Urine Excretion	mRNA Reduction
		μg/ml	*h*μg/ml*	*μg/g*	*h*μg/g*	%	
siRNA12	Sham	0.161	0.501	14.5	ND	42 ng/ml[a]	74
	Nephrectomy	0.131	0.606	14.6	ND	13 ng/ml[a]	73
siRNA14	Sham	0.048	0.198	8.0	752	5	70
	Nephrectomy	0.034	0.139	5.8	765	0.74	70
siRNA5	Sham	0.080	0.303	11.9	ND	3.2	70
	Nephrectomy	0.081	0.300	14.7	ND	1.1	75

[a]Total urine volume not available for normalization.
ND, not determined.

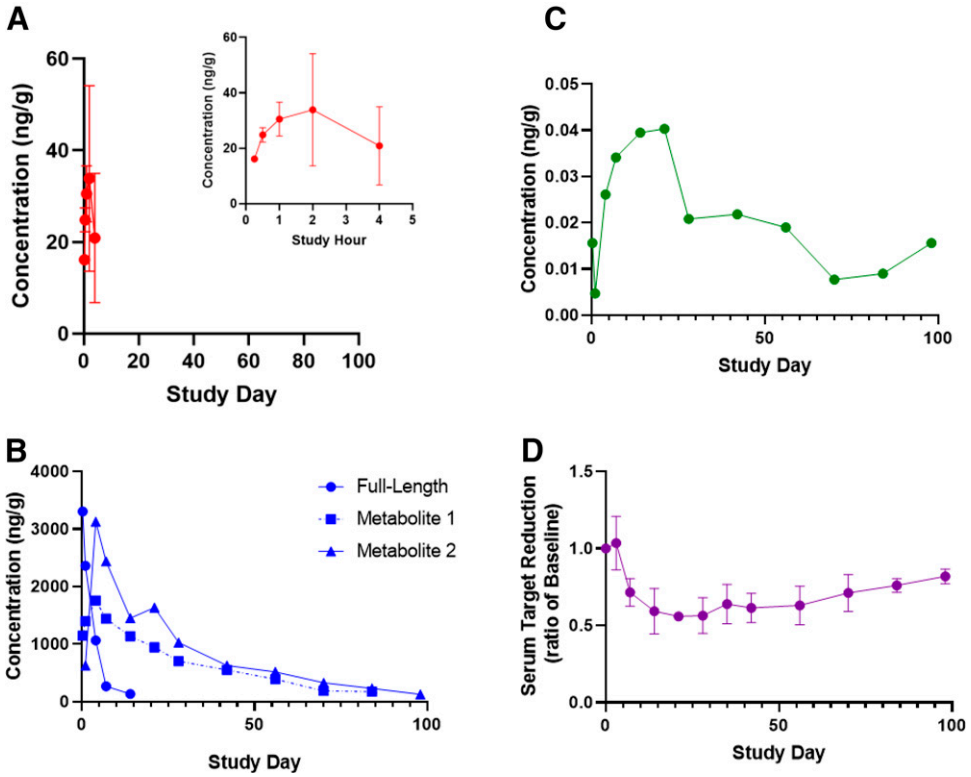

Fig. 8. The time profile (*x*-axis) for concentrations of siRNA17 and two active metabolites was evaluated over 99 days after a single s.c. administration of 3 mg/kg in monkey (n = 3) in plasma (A) (*y*-axis), liver (B) (*y*-axis), and RISC (C) (*y*-axis). In addition, the measurement of target in serum samples was determined using a commercially available ELISA kit to measure pharmacodynamics as a ratio of baseline (predose) levels (D) (*y*-axis). Each point represents the composite mean per time point.

Nonclinical studies in ASGR1 knockout mice confirm that functional ASGPR is required for optimal PD activity of GalNAc-conjugated siRNAs, and in the absence of productive liver uptake, both plasma and kidney exposure increase significantly, as does urinary excretion. Similar observations were made in wild-type mice dosed with the same siRNA containing linker but not GalNAc (Liu et al., submitted manuscript). Previous studies have demonstrated that, despite 50% reduction in ASGPR levels, pharmacodynamic activity is maintained, suggesting that receptor capacity is sufficient to efficiently internalize GalNAc-conjugated siRNA (Willoughby et al., 2018). Although there are literature reports demonstrating relevant changes in hepatic expression of ASGPR in various disease states (Reimer et al., 1991; Matsuzaki et al., 1997; Witzigmann et al., 2016), the data generated to date for liver-directed siRNA support a tiered approach to evaluate the potential impact of hepatic impairment whereby data are first generated in patients with mild hepatic impairment prior to evaluation of PD, safety, and efficacy in moderate and severe hepatic impairment.

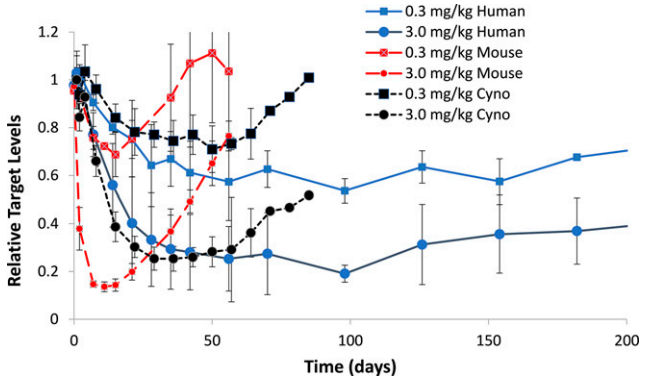

Fig. 9. siRNA7 was administered by a single subcutaneous injection to mouse (red), cynomologus monkey (cyno) (black), and human (blue) at 0.3 (squares) or 3 mg/kg (circle). The extent and duration of target reduction was evaluated through serum measurements over time. The relative target (*y*-axis) over time (*x*-axis) is displayed for n = 3 (mouse and monkey) and n = 6 (human).

The metabolite profile, although slightly different across conjugates, does appear to be well conserved across species, with higher nuclease activity observed in rodents than in monkey and human. In plasma, the current chemical modifications result in limited metabolism overall (<10%) and are similar across conjugates and species. In general, metabolites formed in the liver are expected to contribute to the overall efficacy and are therefore considered in extrapolation of PD from PK.

Excretion data from both radiolabeled and cold studies in rats and monkeys confirm that the majority of the GalNAc-conjugated siRNA is metabolized slowly in liver and excreted as shortmer metabolites through urine and bile. Full-length and truncated metabolites excreted into bile undergo further degradation by endo and exonucleases in the gastrointestinal tract, and shortmer metabolites can be reabsorbed into systemic circulation. An important consideration during clinical development is related to whether renal impairment may impact the pharmacokinetics of the drug, which could lead to higher systemic exposure but no impact on liver uptake or subsequent PD (Wright et al., 2020). Studies in the 5/6 nephrectomy rat model, recapitulating moderate to severe renal impairment, demonstrate that a reduction in urinary excretion does not lead to marked changes in liver PK or observed PD, although transient increases in plasma exposure may be observed. Therefore, renal impairment is unlikely to influence the liver PK and subsequent PD of GalNAc-conjugated siRNAs, and clinical evaluation is often not warranted (Wright et al., 2020).

The PK/PD relationship of GalNAc-conjugated siRNA is more complex than conventional small-molecule drugs. This is exemplified by the delayed onset of action in contrast to the rapid absorption and short plasma half-life observed in nonclinical models and human. Significant understanding has been gained in describing the relationship between dose and exposure in plasma, liver, and RISC using nonclinical models.

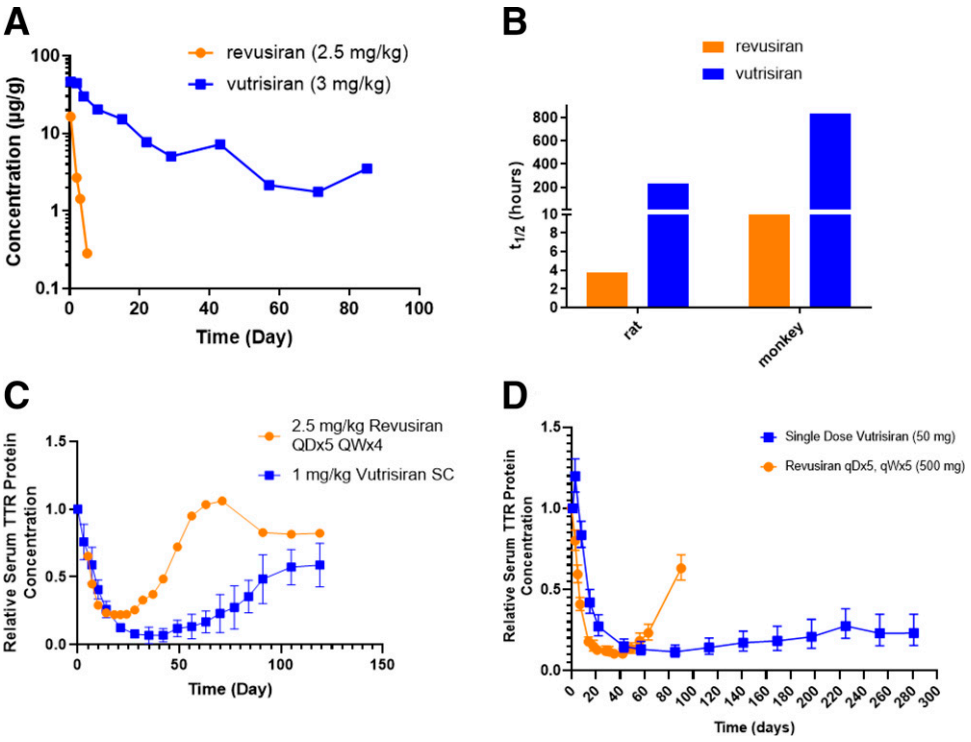

Fig. 10. (A) The concentration (*y*-axis) time profile (*x*-axis) in monkey liver after subcutaneous administration of similar single-dose levels (2.5 mg/kg for revusiran in orange and 3 mg/kg for vutrisiran in blue). (B) The liver half-life values generated from pharmacokinetic data after single-dose administration of revusiran and vutrisiran to rat and monkey. The composite profile of $n = 3$ animals is depicted. (C) The pharmacodynamic activity in monkey ($n = 3$) as relative serum TTR protein level (*y*-axis) over time in days (*x*-axis). Revusiran (orange circles) was given s.c. at 2.5 mg/kg each day for 5 days, followed by weekly dosing for 4 weeks. Vutrisiran (blue squares) was given as a single s.c. injection at 1 mg/kg. (D) The pharmacodynamic activity in human ($n = 6$) as relative serum TTR protein level (*y*-axis) over time in days (*x*-axis). Revusiran (orange circles) was given s.c. at 500 mg each day for 5 days, followed by weekly dosing for 5 weeks. Vutrisiran (blue squares) was given as a single s.c. injection at 50 mg/kg.

It is now recognized that slow release of metabolically stable siRNAs and active metabolites into the cytoplasm from the acidic compartments is key to describing the duration of the PD response. With the success of GalNAc-conjugated siRNAs in treating diseases in the clinic, it is apparent that many of the key ADME properties learned from nonclinical investigations can be translated to predict ADME, liver, and RISC PK in humans.

In summary, the ADME and PK/PD properties of several GalNAc-conjugated siRNAs have been extensively characterized in vitro and in vivo. These data demonstrate that GalNAc-conjugated siRNAs possess ADME and PK/PD properties that are generally well conserved across species, which form the foundation for translation of clinical dose and dosing regimen in the absence of PK and PD data directly derived from human liver. Subcutaneous administration of GalNAc-conjugated siRNAs results in targeted delivery to the intended organ (liver) with a long-lasting PK/PD duration suitable for infrequent dosing in the clinic for this new class of therapeutic modalities.

Acknowledgments

The authors thank the Alnylam In Vivo Sciences and Bioanalytical groups and acknowledge current and former members of the Alnylam Early Development department, the Platform Core Team, and the support of senior management.

Authorship Contributions

Participated in research design: McDougall, Ramsden, Sag. Agarwal, Sak. Agarwal, Brown, Castellanos-Rizaldos, Charisse, Chong, Cichocki, Fitzgerald, Goel, Guenther, Habtemariam, Jadhav, Janas, Jayaraman, Kurz, Li, J. Liu, Maclauchlin, Maier, Manoharan, Nair, Robbie, Smith, Theile, Vaishnaw, Xu, Zlatev, Wu.

Conducted experiments: Ramsden, Sak. Agarwal, Aluri, Arciprete, Brown, Gu, Li, J. Liu, X. Liu, Liou, Manoharan, Schmidt, Theile, Waldron, Zhang.

Performed data analysis: McDougall, Ramsden, Sak. Agarwal, Brown, Castellanos-Rizaldos, Chong, Cichocki, Zhang.

Wrote or contributed to the writing of the manuscript: McDougall, Ramsden, Chong, Fitzgerald, Habtemariam, Jadhav, Maier, Robbie, Zlatev, Wu.

References

Agarwal S, Simon AR, Goel V, Habtemariam BA, Clausen VA, Kim JB, and Robbie GJ (2020) Pharmacokinetics and pharmacodynamics of the small interfering ribonucleic acid, givosiran, in patients with acute hepatic porphyria. *Clin Pharmacol Ther* **108**:63–72.

Agarwal S, Allard R, Darcy J, Chigas S, Gu Y, Nguyen T, Bond S, Chong S, Wu JT, and Janas MM (2021) Impact of serum proteins on the uptake and RNA interference activity of *N*-acetylgalactosamine-conjugated small interfering RNAs. *Nucleic Acid Ther*.

Brown CR, Gupta S, Qin J, Racie T, He G, Lentini S, Malone R, Yu M, Matsuda S, Shulga-Morskaya S, et al. (2020) Investigating the pharmacodynamic durability of GalNAc-siRNA conjugates. *Nucleic Acids Res* **48**:11827–11844.

Carito B, Harbison C, Janas M, and Keirstead N (2016). Targeted delivery of siRNA therapeutics: ASGPR tissue expression evaluation in rat, mouse, and non-human primate. Poster session presented at: *ACVP & ASVCP Concurrent Annual Meeting 2016*; New Orleans, LA.

Castellanos-Rizaldos E, Brown CR, Dennin S, Kim J, Gupta S, Najarian D, Gu Y, Aluri K, Enders J, Brown K, et al. (2020) RT-qPCR methods to support pharmacokinetics and drug mechanism of action to advance development of RNAi therapeutics. *Nucleic Acid Ther* **30**:133–142.

Chen C, Ridzon DA, Broomer AJ, Zhou Z, Lee DH, Nguyen JT, Barbisin M, Xu NL, Mahuvakar VR, Andersen MR, et al. (2005) Real-time quantification of microRNAs by stem-loop RT-PCR. *Nucleic Acids Res* **33**:e179.

Debacker AJ, Voutila J, Catley M, Blakey D, and Habib N (2020) Delivery of oligonucleotides to the liver with GalNAc: from research to registered therapeutic drug. *Mol Ther* **28**:1759–1771.

Fire A, Xu S, Montgomery MK, Kostas SA, Driver SE, and Mello CC (1998) Potent and specific genetic interference by double-stranded RNA in Caenorhabditis elegans. *Nature* **391**:806–811 *Nature.*

Foster DJ, Brown CR, Shaikh S, Trapp C, Schlegel MK, Qian K, Sehgal A, Rajeev KG, Jadhav V, Manoharan M, et al. (2018) Advanced siRNA designs further improve in vivo performance of GalNAc-siRNA conjugates. *Mol Ther* **26**:708–717.

Glund S, Gan G, Moschetti V, Reilly P, Honickel M, Grottke O, and Van Ryn J (2018) The renal elimination pathways of the dabigatran reversal agent idarucizumab and its impact on dabigatran elimination. *Clin Appl Thromb Hemost* **24**:724–733.

Habtemariam BA, Karsten V, Attarwala H, Goel V, Melch M, Clausen VA, Garg P, Vaishnaw AK, Sweetser MT, Robbie GJ, et al. (2021) Single-dose pharmacokinetics and pharmacodynamics of transthyretin targeting N-acetylgalactosamine-small interfering ribonucleic acid conjugate, vutrisiran, in healthy subjects. *Clin Pharmacol Ther* **109**:372–382.

Hail ME, Eliiot B, and Anderson K (2004) High-throughput analysis of oligonucleotides using automated electrospray ionization mass spectrometry. *Am Biotechnol Lab* **22**:12–14 *Am Biotechnol Lab.*

Janas MM, Schlegel MK, Harbison CE, Yilmaz VO, Jiang Y, Parmar R, Zlatev I, Castoreno A, Xu H, Shulga-Morskaya S, et al. (2018) Selection of GalNAc-conjugated siRNAs with limited off-target-driven rat hepatotoxicity. *Nat Commun* **9**:723.

Kliem V, Johnson RJ, Alpers CE, Yoshimura A, Couser WG, Koch KM, and Floege J (1996) Mechanisms involved in the pathogenesis of tubulointerstitial fibrosis in 5/6-nephrectomized rats. *Kidney Int* **49**:666–678.

Kujal P and Vernerová Z (2008). 5/6 Nephrectomy as an experimental model of chronic renal failure and adaptation to reduced nephron number. *Cesk Fysiol* **57**:104–109.

Landesman Y, Svrzikapa N, Cognetta 3rd A, Zhang X, Bettencourt BR, Kuchimanchi S, Dufault K, Shaikh S, Gioia M, Akinc A, et al. (2010) In vivo quantification of formulated and chemically modified small interfering RNA by heating-in-Triton quantitative reverse transcription polymerase chain reaction (HIT qRT-PCR). *Silence* **1**:16.

Li J, Liu J, Enders J, Arciprete M, Tran C, Aluri K, Guan LH, O'Shea J, Bisbe A, Charissé K, et al. (2019) Discovery of a novel deaminated metabolite of a single-stranded oligonucleotide *in vivo* by mass spectrometry. *Bioanalysis* **11**:1955–1965.

Li P, Ma LL, Xie RJ, Xie YS, Wei RB, Yin M, Wang JZ, and Chen XM (2012) Treatment of 5/6 nephrectomy rats with sulodexide: a novel therapy for chronic renal failure. *Acta Pharmacol Sin* **33**:644–651.

Liu J, Li J, Tran C, Aluri K, Zhang X, Clausen V, Zlatev I, Guan L, Chong S, Charisse K, et al. (2019) Oligonucleotide quantification and metabolite profiling by high-resolution and accurate mass spectrometry. *Bioanalysis* **11**:1967–1980.

Matsuzaki S, Onda M, Tajiri T, and Kim DY (1997) Hepatic lobar differences in progression of chronic liver disease: correlation of asialoglycoprotein scintigraphy and hepatic functional reserve. *Hepatology* **25**:828–832.

McDougall R, Ramsden D, Chong S, and Wu J-T (2019). ADME and PK properties of GalNAc-conjugated siRNAs in nonclinical species. High-Throughput ADME Conference (June); Cambridge, MA.

Meister G and Tuschl T (2004) Mechanisms of gene silencing by double-stranded RNA. *Nature* **431**:343–349.

Nair JK, Attarwala H, Sehgal A, Wang Q, Aluri K, Zhang X, Gao M, Liu J, Indrakanti R, Schofield S, et al. (2017) Impact of enhanced metabolic stability on pharmacokinetics and pharmacodynamics of GalNAc-siRNA conjugates. *Nucleic Acids Res* **45**:10969–10977.

Nair JK, Willoughby JLS, Chan A, Charisse K, Alam MR, Wang Q, Hoekstra M, Kandasamy P, Kel'in AV, Milstein S, et al. (2014) Multivalent N-acetylgalactosamine-conjugated siRNA localizes in hepatocytes and elicits robust RNAi-mediated gene silencing. *J Am Chem Soc* **136**:16958–16961.

Ozcan A, Ware K, Calomeni E, Nadasdy T, Forbes R, Satoskar AA, Nadasdy G, Rovin BH, Hebert LA, and Brodsky SV (2012) 5/6 nephrectomy as a validated rat model mimicking human warfarin-related nephropathy. *Am J Nephrol* **35**:356–364.

Ramsden D, Wu JT, Zerler B, Iqbal S, Jiang J, Clausen V, Aluri K, Gu Y, Dennin S, Kim J, et al. (2019) In vitro drug-drug interaction evaluation of GalNAc conjugated siRNAs against CYP450 enzymes and transporters. *Drug Metab Dispos* **47**:1183–1194.

Ray KK, Wright RS, Kallend D, Koenig W, Leiter LA, Raal FJ, Bisch JA, Richardson T, Jaros M, Wijngaard PLJ, et al.; ORION-10 and ORION-11 Investigators (2020) Two phase 3 trials of inclisiran in patients with elevated LDL cholesterol. *N Engl J Med* **382**:1507–1519.

Reimer P, Weissleder R, Lee AS, Buettner S, Wittenberg J, and Brady TJ (1991) Asialoglycoprotein receptor function in benign liver disease: evaluation with MR imaging. *Radiology* **178**:769–774.

Rocca C, Dennin S, Gu Y, Kim J, Chigas S, Najarian D, Chong S, Gutierrez S, Butler J, Charisse K, et al. (2019) Evaluation of electrophoretic mobility shift assay as a method to determine plasma protein binding of siRNA. *Bioanalysis* **11**:1927–1939.

Rudge J, Scott G, Hail M, and Mcginley M (2011) Preparation and LC/MS analysis of oligonucleotide therapeutics from biological matrices. *Chromatography Today* (March):16–20.

Schlegel MK, Foster DJ, Kel'in AV, Zlatev I, Bisbe A, Jayaraman M, Lackey JG, Rajeev KG, Charissé K, Harp J, et al. (2017) Chirality dependent potency enhancement and structural impact of glycol nucleic acid modification on siRNA. *J Am Chem Soc* **139**:8537–8546.

Shen X and Corey DR (2018) Chemistry, mechanism and clinical status of antisense oligonucleotides and duplex RNAs. *Nucleic Acids Res* **46**:1584–1600.

Tapia E, Zatarain-Barrón ZL, Hernández-Pando R, Zarco-Márquez G, Molina-Jijón E, Cristóbal-García M, Santamaría J, and Pedraza-Chaverri J (2013) Curcumin reverses glomerular hemodynamic alterations and oxidant stress in 5/6 nephrectomized rats. *Phytomedicine* **20**:359–366.

Willoughby JLS, Chan A, Sehgal A, Butler JS, Nair JK, Racie T, Shulga-Morskaya S, Nguyen T, Qian K, Yucius K, et al. (2018) Evaluation of GalNAc-siRNA conjugate activity in pre-clinical animal models with reduced asialoglycoprotein receptor expression. *Mol Ther* **26**:105–114.

Witzigmann D, Quagliata L, Schenk SH, Quintavalle C, Terracciano LM, and Huwyler J (2016) Variable asialoglycoprotein receptor 1 expression in liver disease: Implications for therapeutic intervention. *Hepatol Res* **46**:686–696.

Wright RS, Collins MG, Stoekenbroek RM, Robson R, Wijngaard PLJ, Landmesser U, Leiter LA, Kastelein JJP, Ray KK, and Kallend D (2020) Effects of renal impairment on the pharmacokinetics, efficacy, and safety of inclisiran: an analysis of the ORION-7 and ORION-1 studies. *Mayo Clin Proc* **95**:77–89.

Zimmermann TS, Karsten V, Chan A, Chiesa J, Boyce M, Bettencourt BR, Hutabarat R, Nochur S, Vaishnaw A, and Gollob J (2017) Clinical proof of concept for a novel hepatocyte-targeting GalNAc-siRNA conjugate. *Mol Ther* **25**:71–78.

Address correspondence to: Jing-Tao Wu, Drug Metabolism and Pharmacokinetics, Early Development, Alnylam Pharmaceuticals Inc., 675 W Kendall St., Cambridge, MA 02142. E-mail: jtwu@alnylam.com